https://doi.org/10.1016/j.buildenv.2021.107963

Integrated impacts of building height and upstream building on pedestrian comfort around ideal lift-up buildings in a weak wind environment

Lan Chen, Cheuk Ming Mak*

Department of Building Services Engineering, The Hong Kong Polytechnic University, Hung Hom, Hong Kong, China

***Corresponding author: Cheuk Ming Mak**

Email address: cheuk-ming.mak@polyu.edu.hk.

Abstract

Unfavorable wind comfort and intense thermal discomfort are degrading pedestrian comfort in high-density cities. The lift-up design has proved to be a promising way to improve wind comfort and thermal comfort around buildings. Previous studies have identified building height as a crucial factor influencing wind comfort around lift-up buildings. However, the correlation between building height and wind comfort has not been fully understood yet and few parametric studies have been focused on thermal comfort. This study thereby aims to evaluate the integrated effects of building height and upstream building on pedestrian comfort around lift-up buildings from aspects of wind comfort and thermal comfort. Computational fluid dynamics (CFD) simulations were performed to reproduce mean flow fields around single building models and double building models. An integrated method combining on-site observation data and CFD simulation results was employed to calculate physiological equivalent temperatures. The findings show that increasing building height, being under a diverging flow, removing upstream buildings, and making the target building taller or shorter than the upstream building can improve wind comfort in the lift-up area. However, their effects on thermal comfort vary seasonally. For improving wind comfort and thermal comfort in the podium, making the target building taller or shorter than the upstream building or under a diverging flow is beneficial; but increasing building height and removing upstream buildings are not necessarily favorable. The outcome can provide some inspiration for city planners to improve pedestrian comfort in high-density cities.

Keywords: Wind comfort, Thermal comfort, Building height, Lift-up design, Upstream building, CFD simulation

1. Introduction

Nowadays, people's desirability to a livable and sustainable built environment is growing. A suitable neighborhood microenvironment can attract people to enjoy outdoor events at leisure, benefiting their mental and physical health [1]. However, pedestrian comfort is impaired by unfavorable wind comfort and intense thermal discomfort, which overwhelms people's positivity. Modern cities are built towards tall buildings and compact space owing to scarce land resources and increasing city dwellers. The dense layout blocks air circulation in urban areas, causing low wind velocity and unfavorable wind comfort at the pedestrian level [2]. Due to global warming and the urban heat island effect, pedestrians frequently endure severe heat stress and thermal discomfort in summer, especially for tropical and subtropical hot and humid zones. Hong Kong is one of the most densely populated cities globally, with a large number of high-rise buildings. The annual mean wind velocity was steadily decreasing at a rate of 0.2 m/s per decade over urban areas, while it did not vary significantly in rural areas [3]. For pedestrians under shade on a sunny summer day in Hong Kong, obtaining neutral thermal perceptions requires the wind velocity to be at least 1.6 m/s [4]. As wind velocity is an essential factor influencing thermal comfort, weak wind conditions in urban areas can intensify thermal discomfort at the pedestrian level [5]. Therefore, seeking methods to improve pedestrian comfort is of great importance for high-density cities.

Optimizing building design to increase building permeability can improve urban ventilation effectively. Representative building designs include building opening [6-8], arcade [9, 10], and lift-up design [11-16]. As shown in Fig.1(a), the lift-up building generally has open space on the ground floor, formed by using supporting pillars to elevate the main body above the ground. Scientific evidence has confirmed that the lift-up design can improve pedestrian-level wind velocity and wind comfort [11-16], promote ventilation and pollutant dispersion [6, 17-19], and ameliorate thermal comfort [5, 20-22]. Furthermore, the lift-up area can serve as

an entertainment place for pedestrians to relax [11]. Such building design is commonly used in Singapore and southeastern China [12, 13, 16].

(a) (b)

Fig. 1. (a) The lift-up building (photographed by authors) and (b) slab-like building (snapshotted from Google earth) in Hong Kong, China.

Since tall buildings have become common in high-density cities, identifying the correlation between building height and pedestrian comfort is of great significance for applying the lift-up design to practical constructions. For lift-up buildings, modifying building heights can be achieved via changing the main body's height or lifted height, or both. This paper refers to the first type unless otherwise specified. Zhang et al. [23] reported that tall and slender lift-up buildings can cause high wind velocities in lateral and lift-up areas and thus lead to wind discomfort via wind tunnel experiments. Du et al. [7] found that wind comfort around isolated buildings and building groups (3 × 3 arrays) is improved when the target building with lift-up design becomes taller using computational fluid dynamics (CFD) simulations. Another study on building groups (3 × 7 arrays) with lift-up designs shows that the area-weighted average mean wind velocity has a negative correlation (R = -0.58) with the building height [24]. Nevertheless, Chew and Norford [12] studied pedestrian-level wind velocities in 2D street canyons with lift-up design and concluded that near-ground streamwise velocities change

insignificantly with the building height. Further investigation on 3D urban canyons shows that heightening the building from 24m to 48m only increases the overall pedestrian-level streamwise velocity by ~10% [13]. As for thermal comfort, Du et al. [24] found that the correlation value between area-weighted average PET (i.e., physiological equivalent temperature) and building height for building groups (3 × 7 arrays) is -0.14. Hence, it can be concluded that the correlation between building height and wind comfort around lift-up buildings has not been fully explored and understood. Some inconsistent conclusions on the effects of building height on wind comfort have existed. Furthermore, studies on the role of building height on thermal comfort around lift-up buildings are scarce and require more detailed investigations.

Hence, this study aims to provide a comprehensive understanding of the overall effects of building height on pedestrian comfort around lift-up buildings regarding wind comfort and thermal comfort. Single building models were used to examine pedestrian comfort around isolated buildings with three building heights. This study also designed double building models to investigate the effect of building height on pedestrian comfort around the downward lift-up building under the influence of an upstream building. Mean wind velocity ratio (MVR) and PET were adopted as assessment indices for wind comfort and thermal comfort. The validated CFD simulations were employed to predict mean flow fields around buildings. An integrated method combining on-site thermal parameters and CFD predicted wind velocity data [20, 24] was employed to calculate PET values. The novelty of this study can be summarized below: (1) comprehensively considering three issues of building height variation: effects of changing the lift-up building height on pedestrian comfort, effects of changing the upstream building height on pedestrian comfort, and effects of changing heights of upstream and downward buildings synchronously on pedestrian comfort; (2) first performing parametric study on

thermal comfort around lift-up buildings; (3) selecting the slab-like building (Fig. 1(b)) as the target lift-up building model.

The rest of this paper is organized as follows: Section 2 describes the methodology used in this study, including cases description, CFD simulations, and assessment methods; Section 3 presents the validation study of CFD simulations; Section 4 shows all simulation results and discusses the impacts of building height and upstream building on wind comfort and thermal comfort; Section 5 gives the concluding remarks.

2. Methodology

2.1. Cases description

The geometric dimensions of single building models and double building models are depicted in Fig. 2(a). The slab-like building with an included angle of 120° was selected as the target building model, a typical building shape of public rental housing estates in Hong Kong [25]. When the semi-open zone is windward, the wind converges in the near field. In this case, the slab-like building is conceived as being under a converging flow. In contrast, when the semi-open zone is leeward, the wind diverges in the near field; thus, the slab-like building is under a diverging flow. The target building had a plane area of 1344 m^2, lifted above the ground by 3.5 m (h). The main body had three heights (H_T): 50 m, 100 m, and 150 m. As the number and plan area of lift-up pillars can affect the surrounding wind conditions [11, 23, 26], this study adopted the simplification that excluded supporting pillars from the lift-up design [12, 13, 17, 27]. The upstream building was a rectangular-plan building model, 20 m in depth (D_s) and 65 m in width (W_s). The upstream building also had three heights (H_s): 53.5 m (low-rise), 103.5 m (medium-rise), and 153.5 m (high-rise). The distance between the upstream and target buildings (L_s) was 53.5 m. As illustrated in Fig. 2(b), the interest precinct was 150 m long and

150 m wide, consisting of a podium area (marked in pink) and a lift-up area (marked in blue). The lift-up zone's surface facing the approaching flow was defined as the inflow area (marked in orange).

Table 1 summarizes detailed information for all tested cases. For single building models, there were two types of models: SC and SD. SC represents the single building is under a converging flow, while SD means the single building was under a diverging flow. Since all double building models were under a converging flow, they were categorized into three types of models according to the height of the upstream building (H_s). DL represents that the upstream building is a low-rise building with H_s = 53.5 m; DM represents that the upstream building is a medium-rise building with H_s = 103.5 m; DH represents that the upstream building is a high-rise building with H_s = 153.5 m. All tested cases followed the uniform naming standard: case [model type, H_T]. For instance, case [SC, 50] represents the single building model with H_T =50 m is under a converging flow.

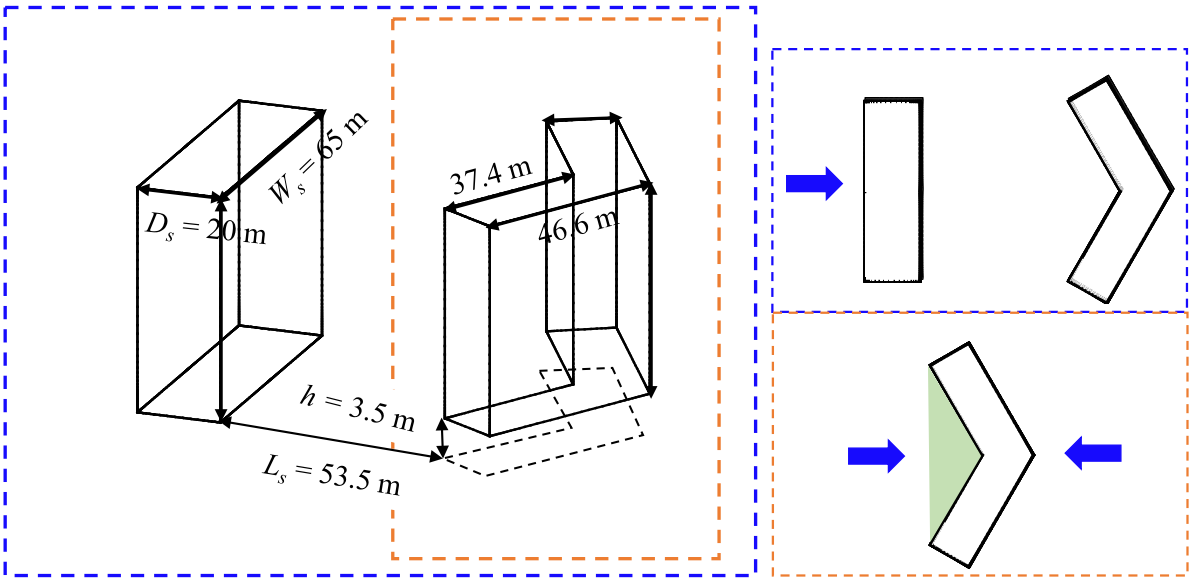

(a)

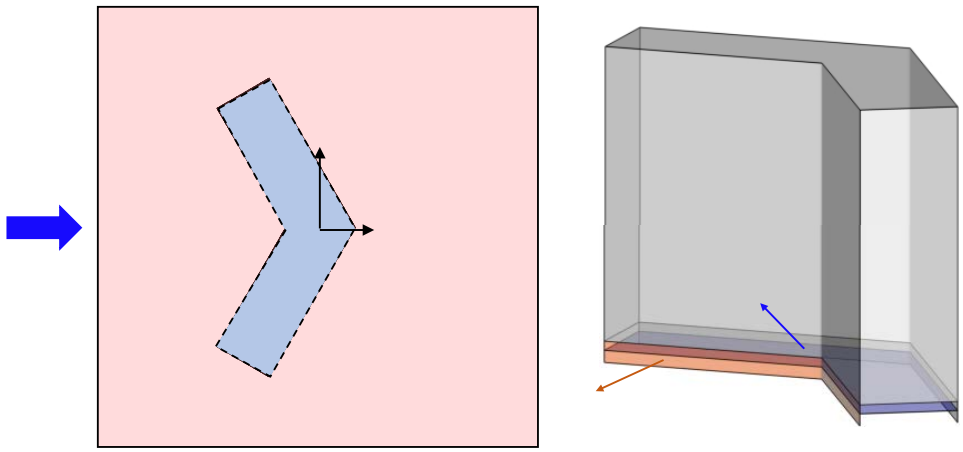

(b)

Fig. 2. Schematic of (a) tested building models and (b) interest areas.

Table 1. Summary of all tested cases.

(a) Single building models (SC and SD)

Case name **Case [model type, H_T]**	**Target building height (H)**		**Remarks**
	Height of main body (H_T)	**Lifted height (h)**	
[SC, 50]	50 m	3.5 m	Under a converging flow
[SC, 100]	100 m	3.5 m	
[SC,150]	150 m	3.5 m	
[SD, 50]	50 m	3.5 m	Under a diverging flow
[SD, 100]	100 m	3.5 m	
[SD, 150]	150 m	3.5 m	

(b) Double building models (DL, DM, and DH)

Case name **Case [model type, H_T]**	**Target building height (H)**		**Upstream building height (H_s)**	**Remarks**
	Height of main body (H_T)	**Lifted height (h)**		
[DL, 50]	50 m	3.5 m	53.5 m	
[DL, 100]	100 m	3.5 m	53.5 m	

[DL, 150]	150 m	3.5 m	53.5 m	A low-rise building upstream
[DM, 50]	50 m	3.5 m	103.5 m	A medium-rise building upstream
[DM, 100]	100 m	3.5 m	103.5 m	
[DM, 150]	150 m	3.5 m	103.5 m	
[DH, 50]	50 m	3.5 m	153.5 m	A high-rise building upstream
[DH, 100]	100 m	3.5 m	153.5 m	
[DH, 150]	150 m	3.5 m	153.5 m	

157

158 **2.2. CFD simulations: computational settings and parameters**

159 **2.2.1. Computational domain and grid arrangement**

160 As using reduced-scale models in CFD simulations of wind-related issues can reduce
161 substantial computation resources without diluting the prediction accuracy [28], this study used
162 the reduced scale ratio (1: 200) of wind-tunnel experiments by Xia et al. [14]. The validation
163 study in Section 3 also adopted the same reduced scale ratio and wind-tunnel data of Xia et al.
164 [14]. The domain size and grid discretization obeyed the best practice guidelines of CFD
165 simulations [29-31]. The computational domain inlet, ceiling, laterals, and outlet were $5H_{max}$,
166 $5H_{max}$, $5H_{max}$, and $15H_{max}$ away from the building models' boundary, respectively, which is
167 illustrated in Fig. 3(a). Here, H_{max} is the bigger one between H and H_s. The x-, y-, and z-
168 coordinate axes denote the streamwise, lateral, and vertical directions. The maximum blockage
169 ratio among all cases was ~2.2%, which is below the recommended threshold value of 3% [29].
170 The domain was discretized into structured hexahedral cells with a minimum grid size of 0.002
171 m. The stretching ratio of adjacent cells was below 1.17. There were five-layer grids from the

ground to the pedestrian level. The total elements were from ~2 million to 5.8 million. Fig. 3(b) shows the grid arrangement of Case [DL, 50].

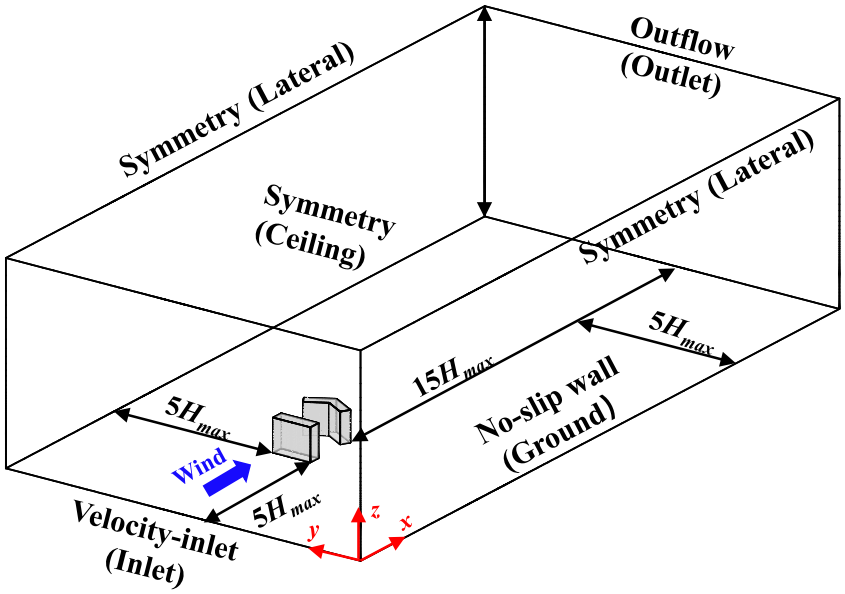

(a)

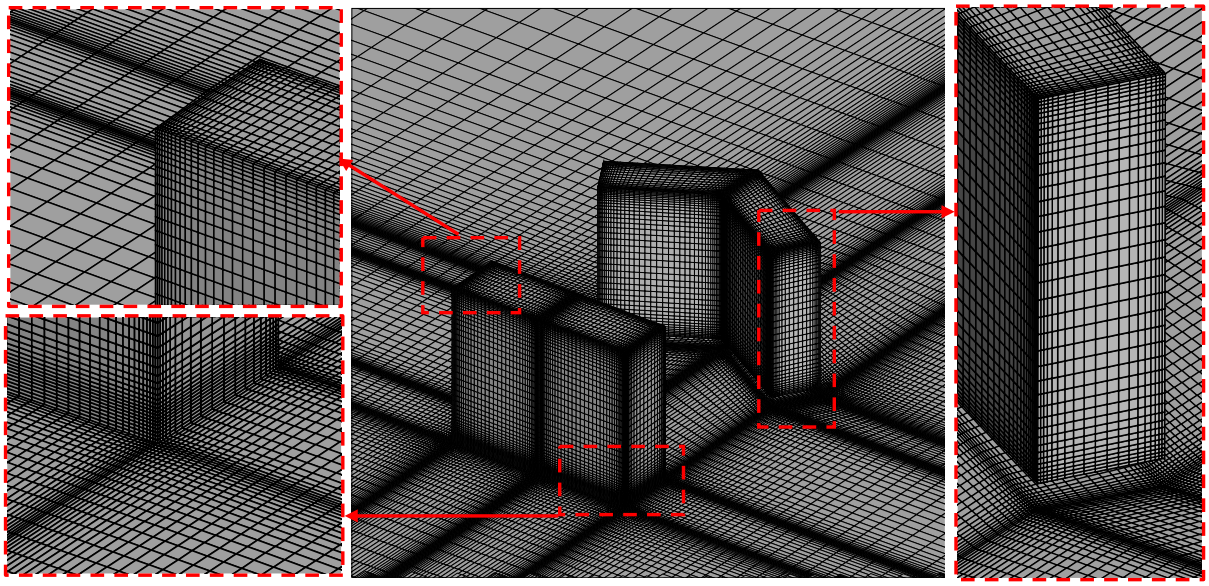

(b)

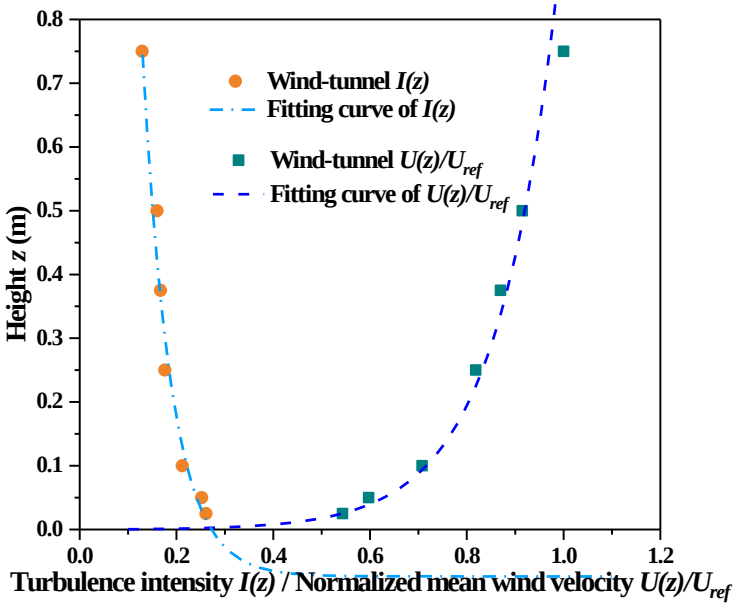

(c)

Fig. 3. Schematics of (a) the computational domain, boundary conditions, and (b) the grid arrangement (Case [DL, 50] as an example); (c) the inlet profiles of turbulence intensity ($I_{(z)}$) and normalized mean wind velocity ($U_{(z)}/U_{ref}$), U_{ref} = 10 m/s is the reference wind velocity at z = 0.75 m [14].

2.2.2. Turbulence model and boundary conditions

The steady Reynolds-averaged Navier-Stokes equations (RANS) with a realizable k-ε turbulence model [32] were employed in CFD simulations due to the intrinsic complexity of mean flow fields in this study. Although large eddy simulations (LES) are inherently superior to RANS in modeling turbulence, RANS methods are used most frequently in urban physics because LES involves complex simulation processes, requires tremendous computational resources, and lacks best practice guidelines [33, 34]. With regard to turbulence closure, the realizable k-ε turbulence model has superior performance in solving complex flow issues involving rotation, separation, recirculation, and strong adverse pressure gradients [32, 35].

Extensive studies have verified the accuracy and reliability of the steady RANS approach with a realizable k-ε turbulence model in modeling mean flows [10, 36-44].

The domain inlet was set as the velocity-inlet boundary condition. The measured turbulence intensity ($I(z)$) and normalized mean wind velocity ($U(z)/U_{ref}$) from wind tunnel experiments of Xia et al. [14] and corresponding fitting curves are shown in Fig. 3(c). The inlet profile of mean wind velocity (U) was obtained by fitting wind tunnel data using Eq. (1) [29]. The inlet turbulence kinetic energy (k) was derived from Eq. (2) by assuming the standard deviations of turbulence fluctuations were equivalent in three directions [43]. The inlet turbulence dissipation rate (ε) was defined by Eq. (3) on the hypothesis of local equilibrium between the turbulence production and dissipation terms [29].

$$U(z) = \frac{u^*}{\kappa} \ln\left(\frac{z+z_0}{z_0}\right), \quad (1)$$

$$k(z) = \frac{3}{2}(I(z)U(z))^2, \quad (2)$$

$$\varepsilon(z) = C_\mu^{\frac{1}{2}} k(z) \frac{dU(z)}{dz}, \quad (3)$$

where, u^* = 0.53 m/s is the frictional velocity ; z_0 = 0.00035 m is the dynamic roughness height; κ = 0.4187 is the von Karman constant; C_μ = 0.09 is the model constant.

The inlet mean wind velocity (U) at z = H was ~8.4 m/s, thus the reference Reynolds number $Re = \frac{UH}{\upsilon} \approx 15 \times 10^4$ (here, υ = 1.46×10^5 m^2/s is the kinematic viscosity coefficient and H = 0.2675 m is the building height). The Re value was beyond the threshold value of 1.5 × 10^4, indicating the flow field satisfies the Re-independent similarity standard [45]. The domain ceiling and laterals were specified as symmetric boundary conditions−zero normal velocity and normal gradients of all variables. The domain outlet was set as the outflow boundary condition, namely zero normal gradients of all variables. The domain ground and building surfaces were

specified as no-slip wall boundary. The average non-dimensional wall distance $y+$ was ~30−40. Thus, the k_s–type standard wall function [46, 47] was utilized for the domain ground. The relationship between k_s and z_0 was determined by Eq. (4) [48], where k_s is the equivalent sand-grain roughness height and C_s is the roughness constant. In this study, k_s was set as 0.00045 m according to the requirement that k_s should not exceed the distance from the center of the wall-adjacent grid to the wall [48].

$$k_s = \frac{9.793 z_0}{C_s}. \quad (4)$$

2.2.3. Solution method

All computations of CFD simulations were accomplished in ANSYS Fluent 13.0 [35]. The SIMPLEC algorithm was selected for pressure–velocity coupling. The finite volume method with the second-order discretization scheme was utilized for discretizing convective and diffusive terms of the governing equations. The under-relaxation factors for the pressure, momentum, k, and ε terms were set as 0.3, 0.7, 0.8, and 0.8, respectively. The iteration computation was considered to reach the convergence when all residual curves approximately stayed stable, and the residuals of the continuity, momentum, k, and ε equations were below 10^{-4}, 10^{-6}, 10^{-6}, and 10^{-5}, respectively.

2.3. Assessment method for wind comfort

Mean wind velocity ratio (MVR) is widely used to evaluate pedestrian-level wind comfort. It is the ratio of local mean wind velocity (U) to the reference mean wind velocity (U_{ref}) (i.e., Eq. (5)) [49]. In this study, U_{ref} was defined as the mean wind velocity at the height of 200 m (in the prototype scale) [16, 23, 26, 50], where the building blocks have negligible effects on

the airflow. Thus, U_{ref} = 10 m/s could be calculated from the inlet wind velocity profile (Eq. (1)).

$$\mathrm{MVR} = \frac{U}{U_{ref}} \tag{5}$$

Du et al. [51] reported wind comfort criteria (e.g. NEN [52]) focusing on solving strong wind issues are not appropriate to the weak wind environment in high-density cities. Therefore, referring to the wind comfort criteria targeting weak wind conditions [23, 51], the mean wind velocity for maintaining an acceptable wind comfort ranges from ~1.5 m/s to 5.3 m/s. As the annual mean wind velocity at the reference height of 200 m in Hong Kong is ~5 m/s [16, 23, 51], the acceptable wind comfort zone requires $0.3 \leq \mathrm{MVR} \leq 1.06$. Thus, areas with MVR < 0.3 are regarded as unfavorable wind comfort zones, while regions with MVR > 1.06 are considered unacceptable wind comfort zones. This classification of wind comfort zones has been used in our previous study [27].

2.4. Assessment method for thermal comfort

PET is used most frequently among over one hundred thermal comfort indices, which is straightforward for laymen [53, 54]. It is based on the Munich Energy-balance model for individuals and defined as the air temperature at which the human heat energy budget is balanced and the human' s skin and core temperatures have equivalent values in the typical indoor environment and the assessed outdoor environment [55]. Different range of PET values indicates different heat/cold stress and thermal perception. This study adopted the modified PET scale for Taiwan to classify thermal sensation and corresponding physiological stress because Hong Kong has a similar humid and hot climate as Taiwan. As shown in Table 2 [56], when the PET value is between 18 and 22, pedestrians feel cool and suffer moderate cold stress.

The calculation of PET was performed using RayMan Pro [57, 58]. An integrated method combing measured heat-related parameters and modeling wind velocities [20, 24] was used to calculate PET values. Liu et al. [20] used this method to predict PET values around an isolated lift-up building and demonstrated its applicability in predicting outdoor thermal comfort at the design stage. Later, Du et al. [24] succeed in applying this integrated method to optimizing pedestrian-level thermal comfort in an ideal urban canyon with lift-up designs. According to this method, the wind velocity for PET calculation was determined by $U_{ref,\,HK} \times$ MVR [59], where $U_{ref,\,HK} = 5$ m/s is the reference mean wind velocity at the height of 200m over Hong Kong [16, 23, 51], and MVR values could be obtained from CFD simulations. Heat-related parameters (i.e., air temperature, humidity, and radiation temperature) and personal information (i.e., clothing insulation) were derived from field surveys. This study referred to meteorological data measured on two sunny days (22 August 2016 and 12 December 2016) at a Hong Kong university campus [22]. Both podium and lift-up areas had a measured site. According to the simultaneous questionnaire survey, the participants' average clothing insulation was ~0.35 clo in summer and ~0.62 clo in winter [21]. The pedestrian was assumed to be a 25-year-old man with 175 cm in height and 70 Kg in weight, standing with a metabolic rate of 1.2 Met [60]. Table 3 summarizes meteorological data and personal information for calculating PET values.

Table 2. PET scales for thermal sensations and physiological stresses in Taiwan [56].

Thermal sensation	**PET range (°C)**	**Physiological stress**
Very cold	≤ 14	Extreme cold stress
Cold	14 − 18	Strong cold stress
Cool	18 − 22	Moderate cold stress
Slightly cool	22 − 26	Slight cold stress
Neutral	26 − 30	No thermal stress
Slightly warm	30 − 34	Slight heat stress

Warm	34 − 38	Moderate heat stress
Hot	38 − 42	Strong heat stress
Very hot	> 42	Extreme heat stress

Table 3. Summary of meteorological parameters and personal information for PET calculations [21, 22].

Variables	**Summer**		**Winter**	
	Podium	**Lift-up area**	**Podium**	**Lift-up area**
Air temperature (°C)	32.8	31.1	25.4	23.6
Relative humidity (%)	86.7	83.0	55.2	61.1
Mean radiant temperature (°C)	58.6	31.6	52.5	23.9
Age	25			
Sex	Male			
Height (m)	175			
Weight (Kg)	70			
Metabolic rate (Met)	1.2			
Clothing insulation (clo)	0.35		0.62	

3. Validation study

3.1. Wind-tunnel model description

Validation data was acquired from wind tunnel experiments conducted by Xia et al. [14] at the Hong Kong University of Science and Technology. Pedestrian-level wind velocities were measured by Irwin probes at the height of 1 cm. The building geometry and dimensions are plotted in Fig. 4(a). The wind-tunnel models were built at a reduced scale of 1: 200. The main body of the building was 25 cm tall (H), 37.5 cm wide (W), and 12.5 cm deep (D). Three lift-up cores had the same dimensions of 4 cm (d) × 4 cm (d) × 1.75 cm (h). The approaching flow

was fully turbulent and normal to the building. More detailed descriptions of wind tunnel experiments can be found in the literature [14, 16, 61].

Fig. 4(b) illustrates the computational domain and boundary conditions in the validation study. The *x*-, *y*-, and *z*-coordinate axes indicate the streamwise, lateral, and vertical directions. The numerical models had the same reduced scale ratio as wind-tunnel models. The distances between the building and the domain inlet, domain ceiling, domain outlet, and domain laterals were 5*H*, 5*H*, 5*H*, and 15*H*, respectively, which conforms to the best practice guidelines of CFD simulations [29-31]. Three structured hexahedral grid arrangements with minimum grid sizes of 1, 2, and 4 mm were constructed to perform the grid sensitivity test, which is shown in Fig. 4(c). The total elements for coarse, medium and fine grid arrangements were about 1 million, 2.1 million, and 3.6 million, respectively. The turbulence model, discretization method, boundary conditions, wall function, solution methods, and convergence criterion used in the validation study agreed with tested cases described in subsection 2.2.

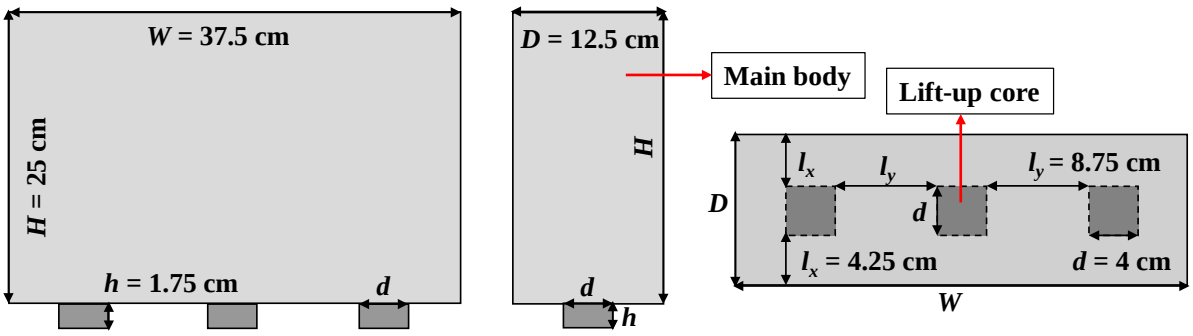

(a)

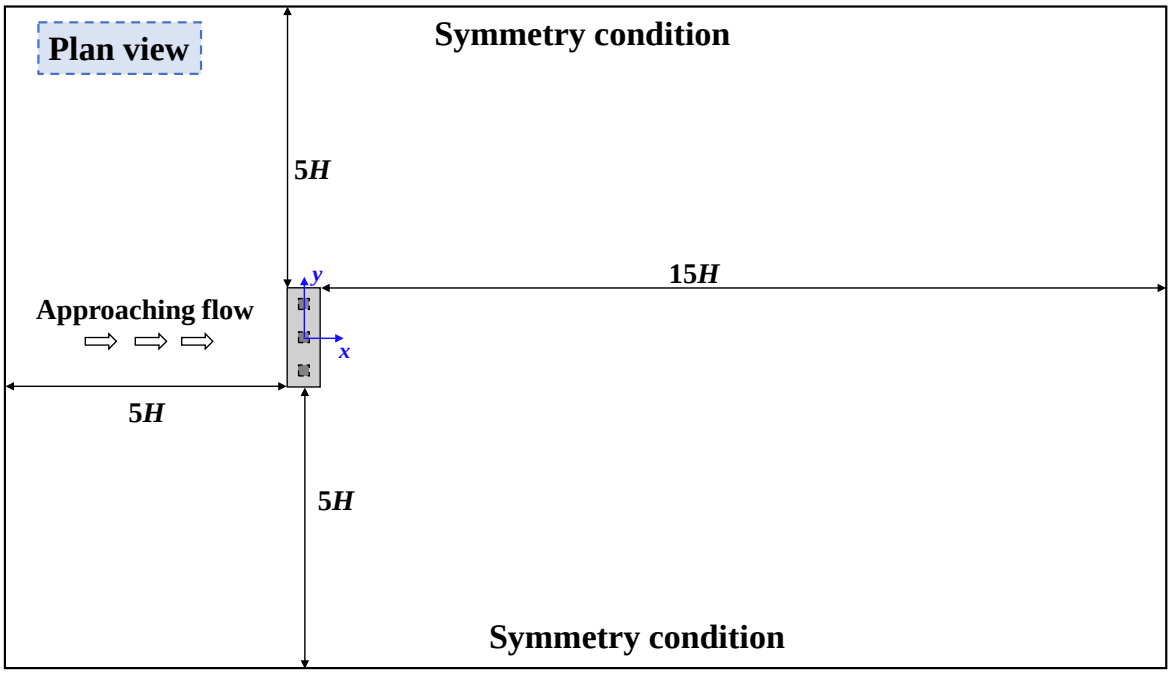
Plan view
Symmetry condition
5H
15H
y
x
Approaching flow
5H
5H
Symmetry condition

305

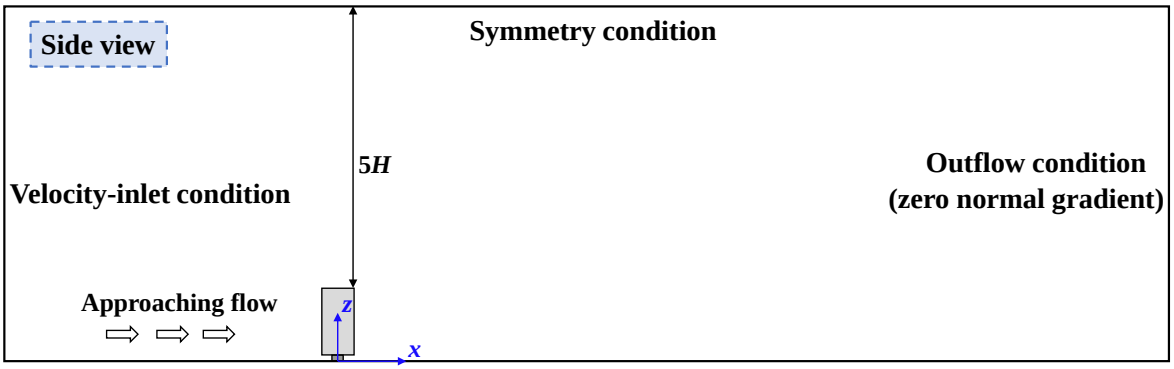
Side view
Symmetry condition
5H
Velocity-inlet condition
Outflow condition
(zero normal gradient)
Approaching flow
z
x

306

307 (b)

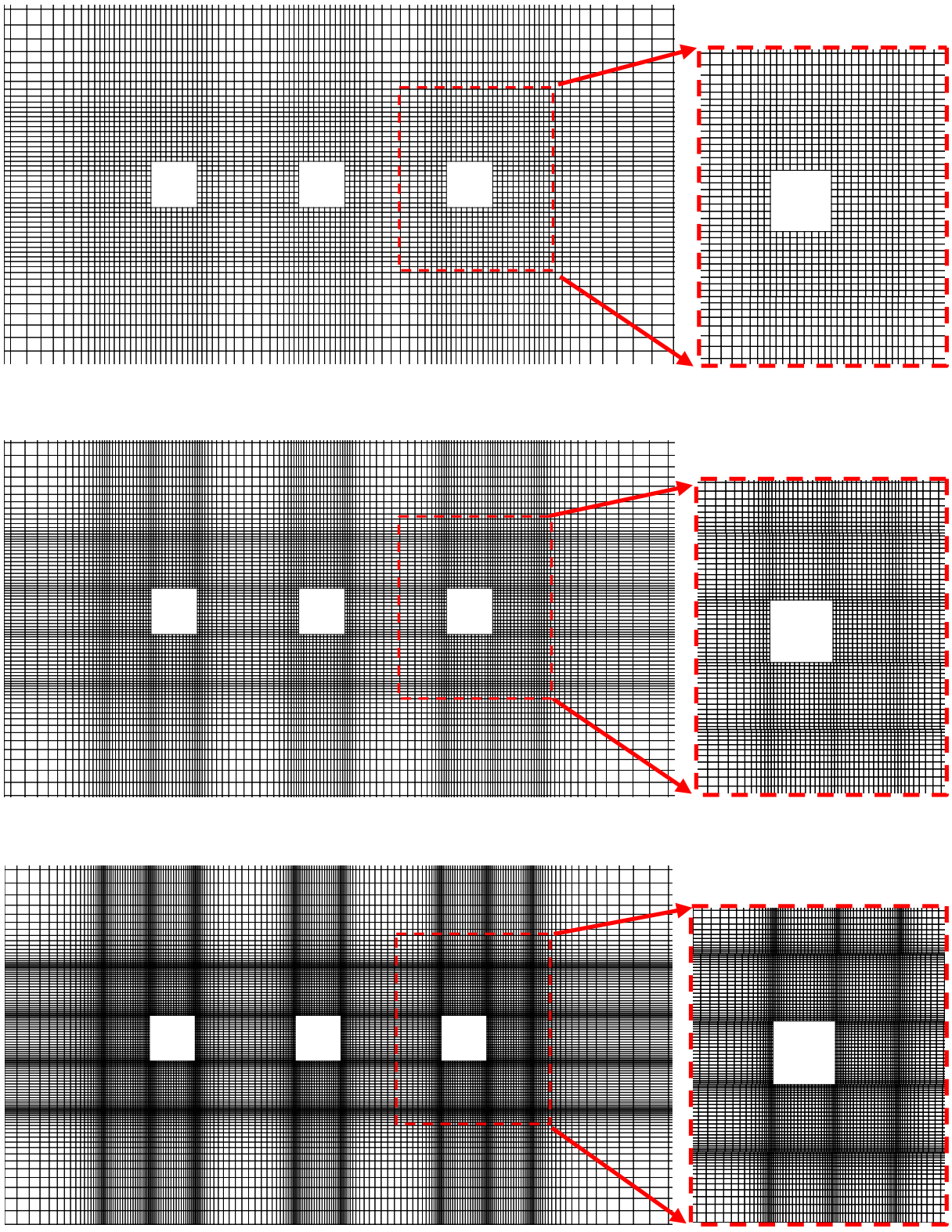

(c)

Fig. 4. (a) Building geometry and dimensions, (b) computational domain and boundary conditions, and (c) coarse, medium, and fine grid arrangements (the domain ground) in the validation study.

3.2. Validation results

Fig. 5 compares wind-tunnel and simulated $U(z)/U_{ref}$ at three horizontal lines (x = -0.25H, 2H, and 3.25H). U_{ref} represents the reference wind velocity at the height of z = 0.75 m. The results show that medium and fine grid arrangements have little difference in predicting mean wind flow, which implies the medium grid arrangement can reproduce the grid-independence flow field. Furthermore, simulated results have good consistency with the wind-tunnel data in most cases. Large deviations over 50% occur in the wake region (x = 3.25H) because the steady RANS approach cannot predict vortex shedding in the wake region [38, 62-64]. The correlation coefficient (R), the fraction bias (FB), the normalized mean square error (NMSE), and the fraction of predictions within a factor of two of observation (FAC2) were calculated to quantify the discrepancy between wind-tunnel data and simulated results of medium grid arrangements. The values of four statistical metrics for three horizontal lines of medium grid arrangements are presented in Table 4. According to the recommended criteria in literature [65-67], a satisfactory prediction requires R > 0.8, |FB| < 0.3, NMSE < 4, and FAC2 > 0.5. As shown in Table 4, all values of R are over 0.97, which indicates that prediction results are highly related to wind tunnel data. The positive FB values represent that CFD simulations generally underestimate velocity magnitudes. Since values of NMSE and FB are rather low (below 0.07), overall prediction errors are small and acceptable. As the values of R, FB, NMSE, and FAC2 meet the recommended criteria [65-67], the employed CFD model with medium grid arrangements could predict the mean flow field with sufficient accuracy.

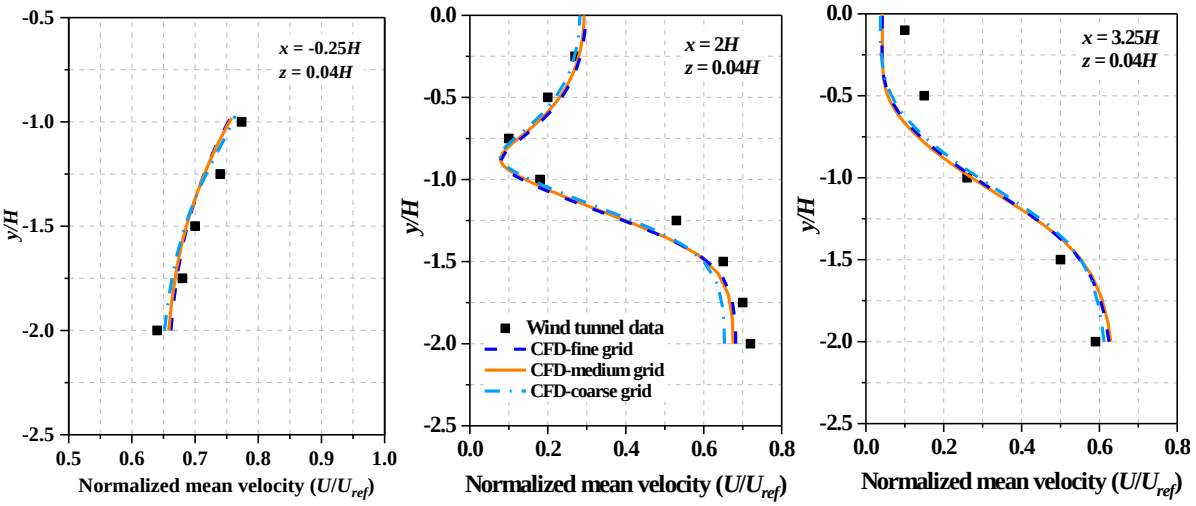

(a) (b) (c)

Fig. 5. Comparison of $U(z)/U_{ref}$ values at lines (a) x = -0.25H, (b) x = 2H, and (c) x = 3.25H between wind-tunnel data and CFD simulation results.

Table 4 Summary of validation metrics for $U(z)/U_{ref}$ values of medium grid arrangements.

Statistics metrics	Recommended criteria [65-67]	x = -0.25H Fig. 5(a)	x = 2H Fig. 5(b)	x = 3.25H Fig. 5(c)
R	> 0.8	0.971	0.984	0.993
FB	- 0.3 – 0.3	0.015	0.068	0.027
NMSE	< 4	0.0007	0.019	0.031
FAC2	> 0.5	1	1	0.6

4. Results and discussion

4.1. Impacts of building height on wind comfort for isolated buildings

4.1.1. Areas of wind comfort zones

Fig. 6 shows pedestrian-level MVR distributions around isolated buildings with different building heights (H_T = 50 m, 100m, and 150 m, in the prototype scale). The interest precinct is

where the black dashed line encircles, and the lift-up building is where the bold black line surrounds. It can be observed that pedestrian-level wind condition around and underneath the isolated building varies with the building height. Whether the building is under a converging flow or a diverging flow, more high wind velocity (MVR > 0.7) zones occur in the lateral and lift-up areas as the building becomes higher. It means that corner streams in the lateral areas and throughflow in the lift-up area strengthen notably with building height. This phenomenon can be attributed to the enhanced downwash along the windward facade due to the building heightening [68]. Similar phenomena are also reported in the literature [7, 23, 26], where rectangular- or square- plan building models elevated off the ground by pillars were adopted. On the other hand, when the building height increases, the upstream unfavorable wind comfort zone (MVR < 0.3) stretches upstream, and downstream unfavorable wind comfort zone moves downstream.

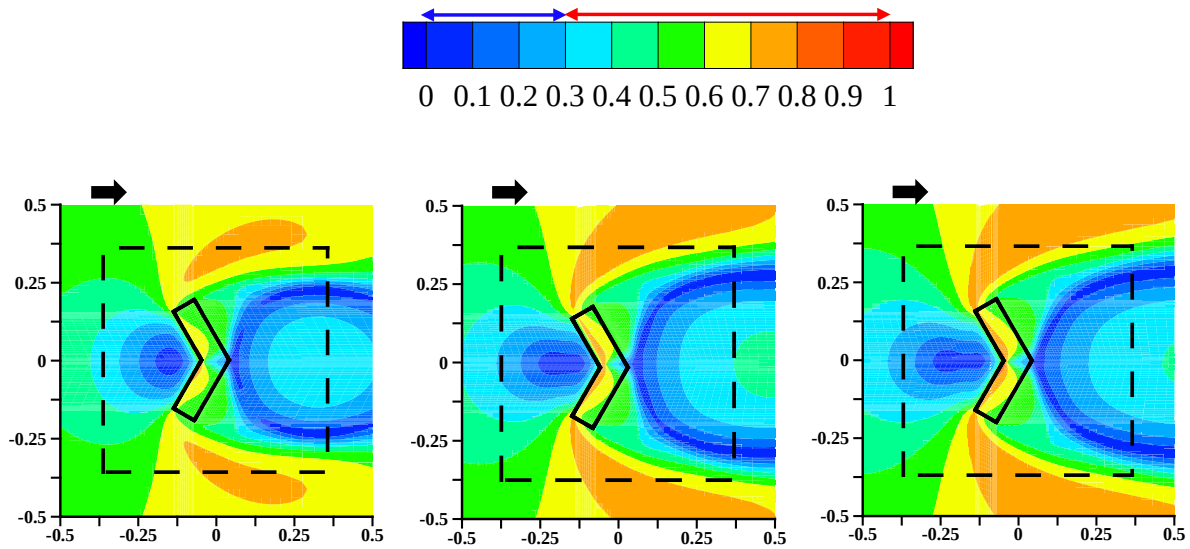

(a) (b) (c)

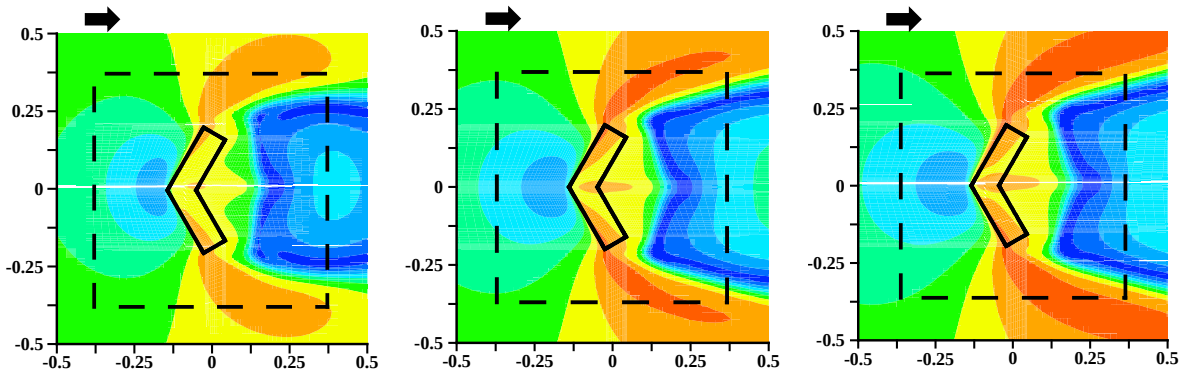

(d) (e) (f)

Fig. 6. Pedestrian-level MVR distributions around isolated buildings with different building heights (H_T = 50 m, 150 m, and 150 m, in the prototype scale): (a-c) is under a converging flow; (d-f) is under a diverging flow; the coordinate axis is scaled by 1: 200; the interest precinct is where the black dashed line encircles and the target building's lift-up area is where the black bold line surroundings.

Area ratios of upstream and downstream unfavorable wind comfort zones (AR_{UFWC}) and overall acceptable wind comfort zone (AR_{AWC}) for single building models are compared in Fig. 7. The upstream AR_{UFWC} is defined as a ratio of the area of the upstream unfavorable wind comfort zone (A_{UFWC}) to the area of the interest precinct (A_T) (Eq. (7)). Similarly, the downstream AR_{UFWC} equals the area of the downstream unfavorable wind comfort zone divided by A_T (Eq. (7)). AR_{AWC} is equal to the area of the overall acceptable wind comfort zone in the podium (A_{AWC}) divided by A_T (Eq. (8)).

$$AR_{UFWC} = \frac{A_{UFWC}}{A_T} \tag{7}$$

$$AR_{AWC} = \frac{A_{AWC}}{A_T} \tag{8}$$

Quantitatively, the upstream AR_{UFWC} value in the podium is augmented by approximately 35% under a converging flow and 92.3% under a diverging flow when the building height triples (Fig. 7(a)). In contrast, the downstream AR_{UFWC} values' variation amplitude is not as

significant as the upstream one. The downstream AR_{UFWC} value increases by about 21.6% under a converging flow but varies little under a diverging flow (Fig. 7(b)). As a result, the decline of AR_{AWC} value is within 10% under both converging and diverging flows when heightening the building from 50 m to 150 m (Fig. 7(c)). Zhang et al. [23] found that when the building gets taller, the upstream low wind speed zone expands slightly, but the downstream near-field low wind speed zone shrinks. Du et al. [7] reported that the upstream unfavorable wind comfort zone decreases but the downstream unfavorable wind comfort zone increases with building height. The differences may be caused by different sizes of interest precincts and building models.

To sum up, for isolated lift-up buildings, high-rise buildings cause a slightly smaller acceptable wind comfort zone in the podium than low-rise ones, although they generate stronger corner streams and throughflow.

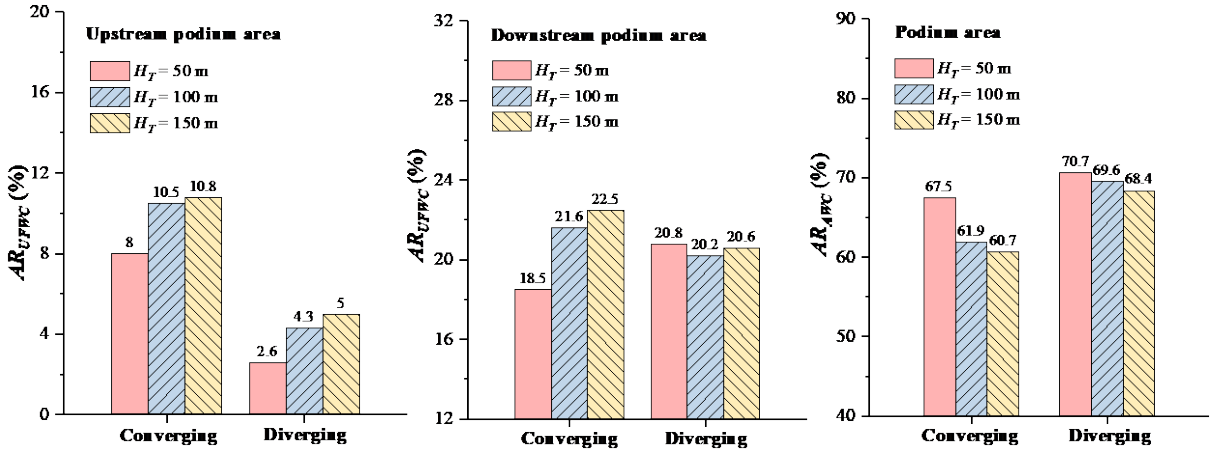

(a) (b) (c)

Fig. 7. Area ratios of (a-b) upstream and downstream unfavorable wind comfort zones (AR_{UFWC}) and (c) overall acceptable wind comfort zone (AR_{AWC}) in the podium for all single building models.

4.1.2. Area-weighted average velocity

Fig. 8(a-b) shows area-weighted average w/U_{ref} and u/U_{ref} values of the inflow area ($\overline{w/U_{ref}}, \overline{u/U_{ref}}$) for all single building models, where w is the vertical velocity and u is the streamwise velocity. The negative value of $\overline{w/U_{ref}}$ indicates that the wind is downward and the positive value of ($\overline{u/U_{ref}}$) represents the wind is streamwise or downstream. As the building gets higher, the magnitudes of $\overline{w/U_{ref}}$ and $\overline{u/U_{ref}}$ are increased. To some extent, this finding demonstrates that the downwash along the windward facades strengthens with the building height. As a result, the area-weighted average MVR ($\overline{\text{MVR}}$) of the lift-up area increases significantly with the building height, as shown in Fig. 8(c). In contrast, the $\overline{\text{MVR}}$ value of the podium area fluctuates flatter. Compared to low-rise buildings, high-rise buildings tend to have a higher $\overline{\text{MVR}}$ value of the podium area under a diverging flow but a lower one under a converging flow.

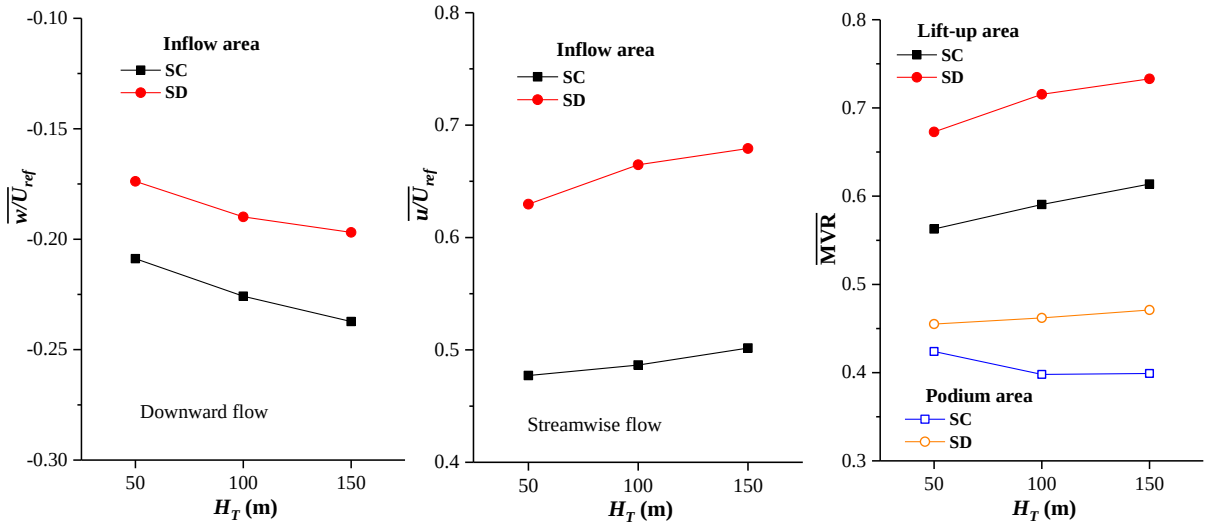

(a) (b) (c)

Fig. 8. Area-weighted average (a) w/U_{ref} ($\overline{w/U_{ref}}$) and (b) u/U_{ref} ($\overline{u/U_{ref}}$) of the inflow area, and (c) area-weighted average MVR ($\overline{\text{MVR}}$) of the podium and lift-up areas for single building models.

4.1.3. Influence of converging and diverging flow

As depicted in Figs. 6 and 7, Case [SC, 50], Case [SC, 100], and Case [SC, 150] have larger upstream AR_{UFWC} values and weaker corner streams than Case [SD, 50], Case [SD, 100], and Case [SD, 150]. Case [SC, 50] has a slightly smaller downstream AR_{UFWC} value than Case [SD, 50], while Case [SC, 100] and Case [SC, 150] have tiny greater downstream AR_{UFWC} values than Case [SD, 100] and Case [SD, 150]. Overall, cases under a diverging flow have greater AR_{AWC} values than cases under a converging flow. From the perspective of velocity magnitude (Fig. 8), cases under a diverging flow have greater $\overline{\mathrm{MVR}}$ values of the podium area than cases under a converging flow. Besides, although cases under a converging flow have greater absolute values of $\overline{w/U_{ref}}$, cases under a diverging flow have much larger $\overline{u/U_{ref}}$ values. As a result, cases under a diverging flow have greater $\overline{\mathrm{MVR}}$ values of the lift-up area than cases under a converging flow. It can be concluded that lift-up buildings cause better wind comfort under a diverging flow, and this phenomenon does not vary with building heights.

4.2. Integrated impacts of building height and upstream building on wind comfort

4.2.1. Areas of wind comfort zones

Pedestrian-level MVR distributions around target buildings under the influence of upstream buildings are presented in Fig. 9. The interest precinct around the target building is encircled by the red dashed line. The white rectangular circled by the black line represents the upstream building. The target building's lift-up area is where the black bold line surroundings. Fig. 10 shows the change of AR_{UFWC} and AR_{AWC} values among all double building models.

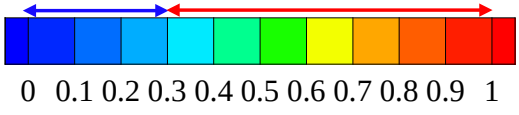

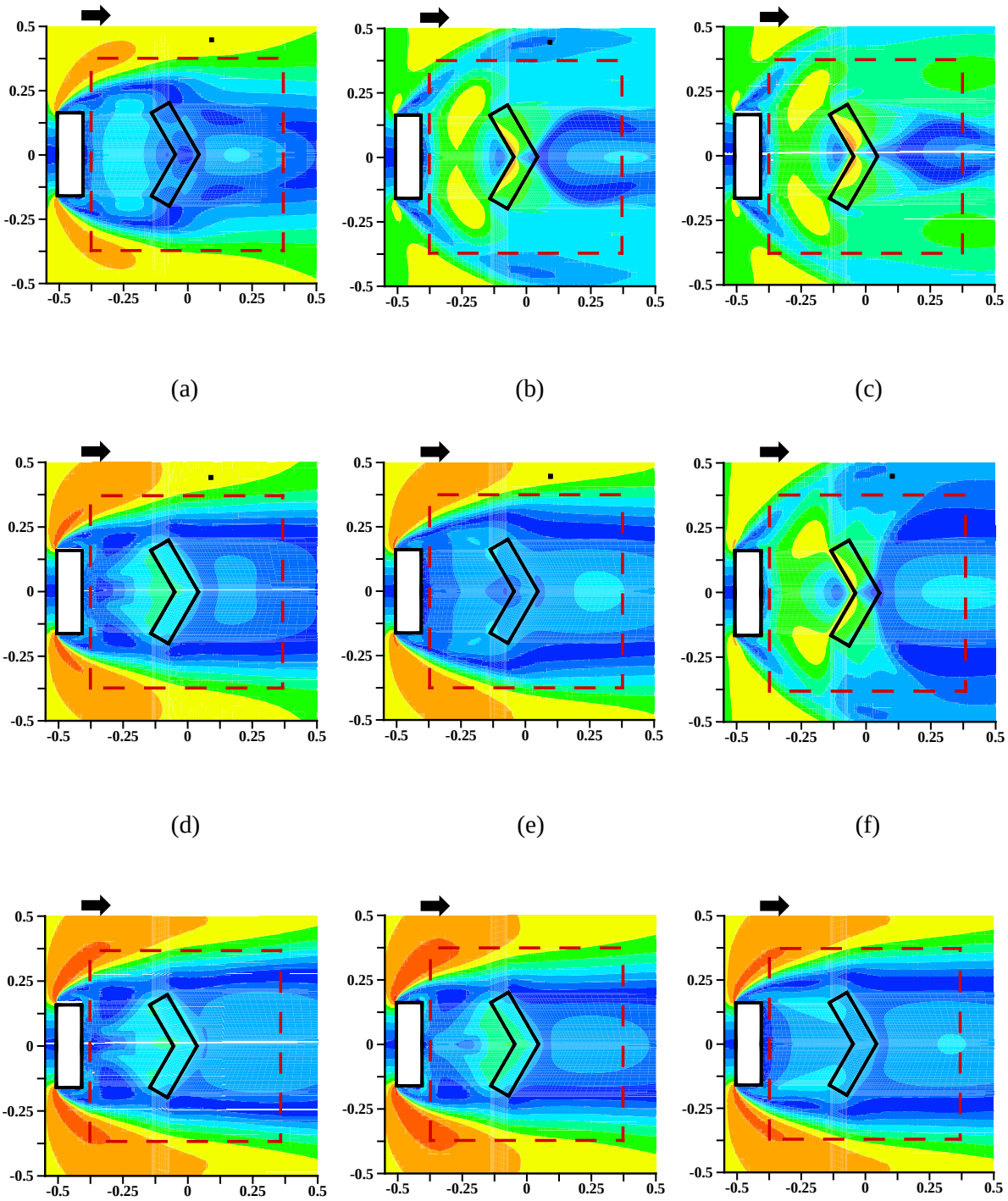

(a) (b) (c)

(d) (e) (f)

(g) (h) (i)

Fig. 9. Pedestrian-level MVR distributions around target buildings under the influence of upstream buildings: (a-c) are cases of DL models (H_s = 53.5 m, in the prototype scale); (d-f) are cases of DM models (H_s = 103.5 m); (g-i) are cases of DH models (H_s = 153.5 m); the coordinate axis is scaled by 1: 200; the interest precinct is where the red dashed line encircles; the upstream building is the white

rectangular circled by black bold lines and the target building's lift-up area is where the black bold line surroundings.

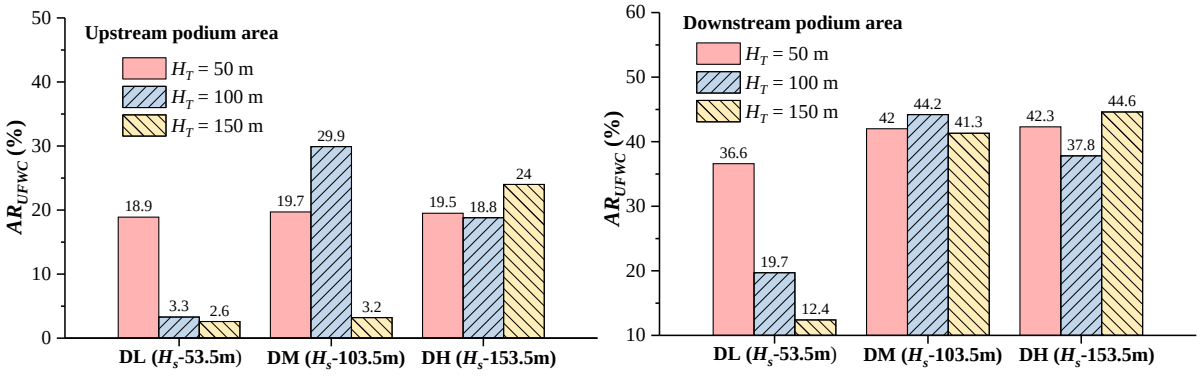

(a) (b)

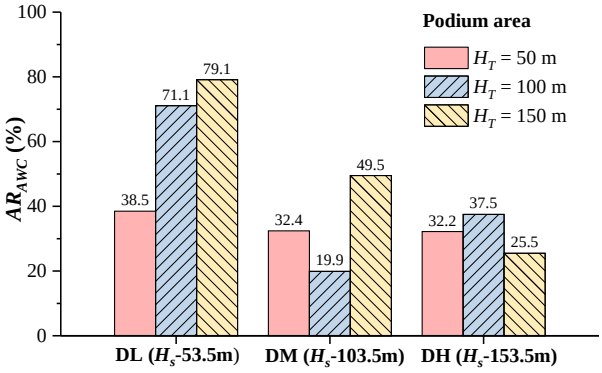

(c)

Fig. 10. Area ratios of (a) upstream AR_{UFWC}, (b) downstream AR_{UFWC}, and (c) overall AR_{AWC} values in the podium for double building models.

For cases of DL models (H_s = 53.5 m, Fig. 9(a-c)), the unfavorable wind comfort zone in the podium dramatically shrinks as the target building height (H_T) increases. Furthermore, the throughflow in the lift-up area strengthens with the increasing target building height, and thus the acceptable wind comfort zone in the lift-up area continuously enlarges. Quantitatively, upstream and downstream AR_{UFWC} values are augmented by about seven times and three times, respectively, when the target building height drops from 150 m to 50 m (Fig. 10(a-b)).

Consequently, the overall AR_{AWC} value of Case [DL, 150] is over twice that of Case [DL, 50] (Fig. 10(c)).

For cases of DM models (H_s = 103.5 m, Fig. 9(d-f)), Case [DM, 150] has the smallest unfavorable wind comfort zone in the entire interest precinct; followed by Case [DM, 50]; Case [DM, 100] has the largest one. Specifically, changing the target building height modifies wind comfort mainly in the upstream and lift-up areas. As shown in Fig. 10, the downstream AR_{UFWC} value varies little (from ~41% to 44%) among three target building heights, while the upstream AR_{UFWC} value changes remarkably (from ~3% to 30%). As for the acceptable wind comfort zone in the podium, the AR_{AWC} value of Case [DM, 150] is about 2.5 times that of Case [DM, 100], and the AR_{AWC} value of Case [DM, 50] is about 63% smaller than that of Case [DM, 150].

For cases of DH models (H_s = 153.5 m, Fig. 9(g-i)), the unfavorable wind comfort zone dominates the entire interest precinct. As presented in Fig. 10, Case [DH, 150] has the maximum upstream and downstream AR_{UFWC} values and the minimum AR_{AWC} value. Case [DH, 100] and Case [DH, 50], in which the target building is shorter than the upstream building, have greater AR_{AWC} values. This finding indicates that reducing the target building height can improve wind comfort around and underneath the target lift-up building when there is a high-rise upstream. Nevertheless, it does not mean the lower the better, as Case [DH, 50] has a smaller AR_{AWC} value than Case [DH, 100].

In summary, cases of $H_s = H_T + h$ (i.e., Case [DL, 50], Case [DM, 100], and Case [DH, 150]) always have the smallest acceptable wind comfort zone in the entire interest precinct among cases with the same H_s. Therefore, when there is a building upstream, making the target lift-up building higher or lower than the upstream building can effectually increase the acceptable wind comfort zone. Comparing case [DL, 100], case [DL, 150], and case [DM, 150], it can be found that when the target building is taller than the upstream building ((H_T +

485 $h)/H_s$ >1), the AR_{AWC} value increases with the value of $(H_T + h)/H_s$. For case [DM, 50], case
486 [DH, 50], and case [DH, 100], in which the target building is lower than the upstream building
487 ($(H_T + h)/H_s$ <1), their AR_{AWC} values also display a rising trend with the $(H_T + h)/H_s$ value.
488 Furthermore, cases of $(H_T + h)/H_s$ >1 have greater AR_{AWC} values than cases of $(H_T + h)/H_s$ <1.
489 Therefore, the target building with a bigger $(H_T + h)/H_s$ value tends to form a larger acceptable
490 wind comfort zone in the podium than the one with a smaller $(H_T + h)/H_s$ value, on the premise
491 that these target buildings are not as tall as upstream buildings. Besides, heightening the target
492 building increases the acceptable wind comfort zone more effectively than shortening the target
493 building.

494

495 **4.2.2. Area-weighted average velocity**

496 Fig. 11(a-b) shows area-weighted average w/U_{ref} and u/U_{ref} ($\overline{w/U}_{ref}$ and $\overline{u/U}_{ref}$)
497 values of the inflow area for double building models. For cases of $(H_T + h)/H_s$ >1, there is a
498 negative $\overline{w/U}_{ref}$ value and a positive $\overline{u/U}_{ref}$ value, which indicates that the wind flowing
499 through the inflow area is downward and streamwise. On the contrary, cases of $(H_T + h)/H_s$ <1
500 have a positive $\overline{w/U}_{ref}$ value and a negative $\overline{u/U}_{ref}$ value. It suggests that the wind flowing
501 through the inflow area is upward and upstream. In other words, the "inflow area" turns to an
502 "outflow area." For cases of $(H_T + h)/H_s$ =1, the $\overline{u/U}_{ref}$ value is also negative but the $\overline{w/U}_{ref}$
503 value depends on the building height. Case [DL, 50] has a negative $\overline{w/U}_{ref}$ value, while Case
504 [DM, 100] and Case [DH, 150] have positive values.

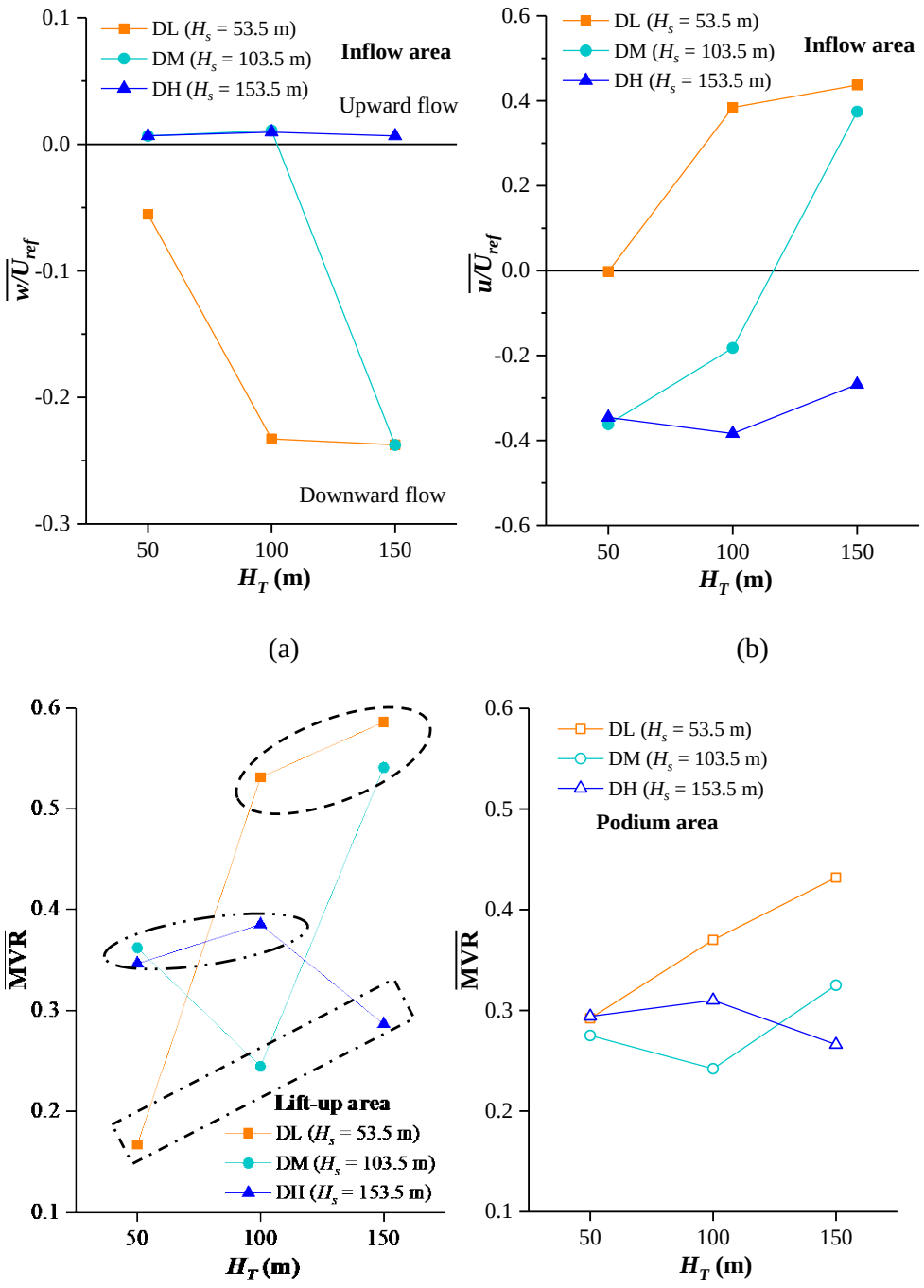

Fig. 11. (a-b) Area-weighted average w/U_{ref} ($\overline{w/U}_{ref}$) and u/U_{ref} ($\overline{u/U}_{ref}$)values of the inflow area and (c-d) area-weighted average MVR ($\overline{\text{MVR}}$) of the podium and lift-up areas for double building models (H_T and H_s values are in the prototype scale).

The distribution of MVR values and streamlines at the vertical plane of y = 0 for cases of different (H_T + h)/H_s values is depicted in Fig. 12. For Case [DL, 150], the downward flow

along the target building's windward facade is strong enough to flow through the lift-up area, even causing a small anti-clockwise turbulence vortex behind the target building. The throughflow in the lift-up area is thereby derived from the downward flow and streamwise, similar to cases of single building models. For Case [DH, 100] and Case [DH, 150], the wind along the target building's windward facade is relatively weak; thus, the throughflow in the lift-up area originates from the reverse flow and is upstream. Such upstream throughflow contributes to the formation of upstream acceptable wind comfort zones in cases of $(H_T + h)/H_s$ <1, as shown in Fig. 9(d, g, h). For Case [DL, 50], the streamwise flow arising from the downwash encounters the reverse flow in the lift-up area, thus forming extremely weak wind velocities (shown in Fig. 9(a)). Comparing case [DL, 150] and case [DL, 50], it can be found that wind velocities in the central street canyon between two buildings are remarkably increased by heightening the target building. In contrast, shortening the target building improves the wind condition mainly near the ground (case [DH, 100] and case [DH, 150]). To some extent, this can explain why heightening the target building is more effective than shortening the target building in improving wind comfort.

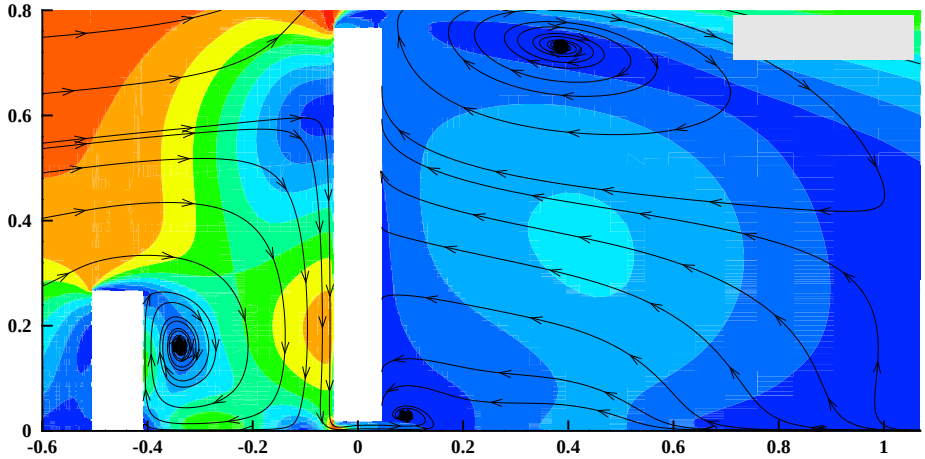

(a)

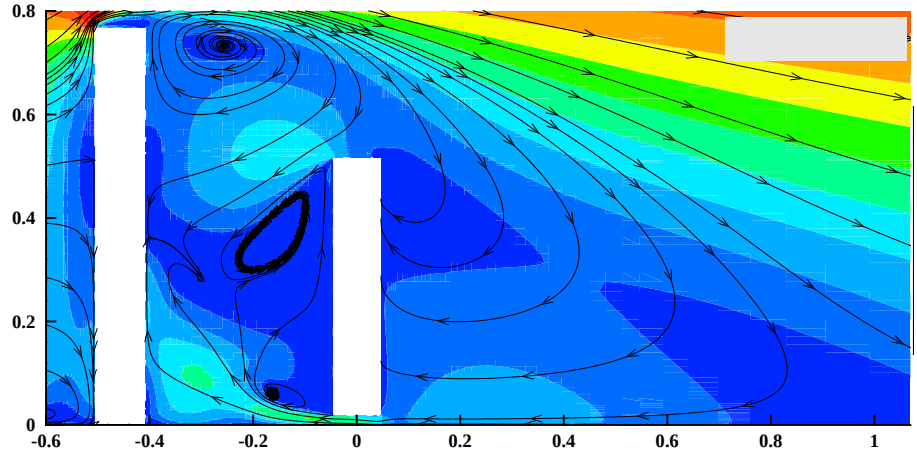
0.8
0.6
0.4
0.2
0
-0.6
-0.4
-0.2
0
0.2
0.4
0.6
0.8
1

(b)

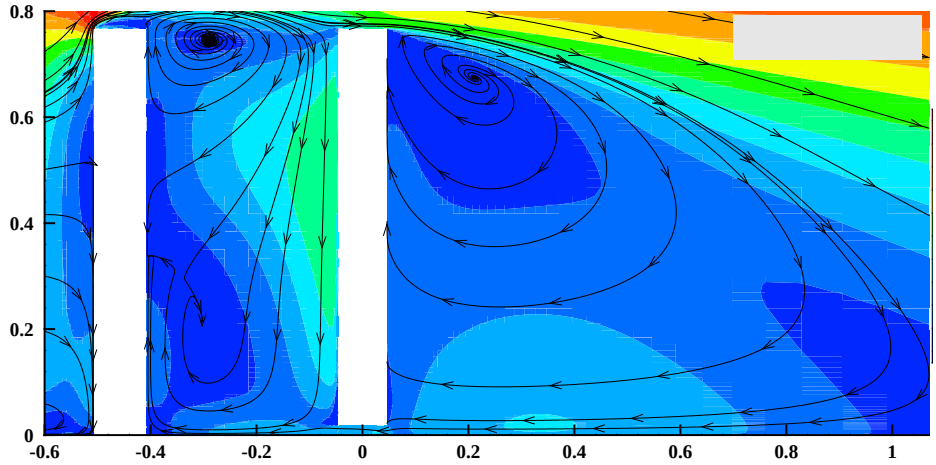
0.8
0.6
0.4
0.2
0
-0.6
-0.4
-0.2
0
0.2
0.4
0.6
0.8
1

(c)

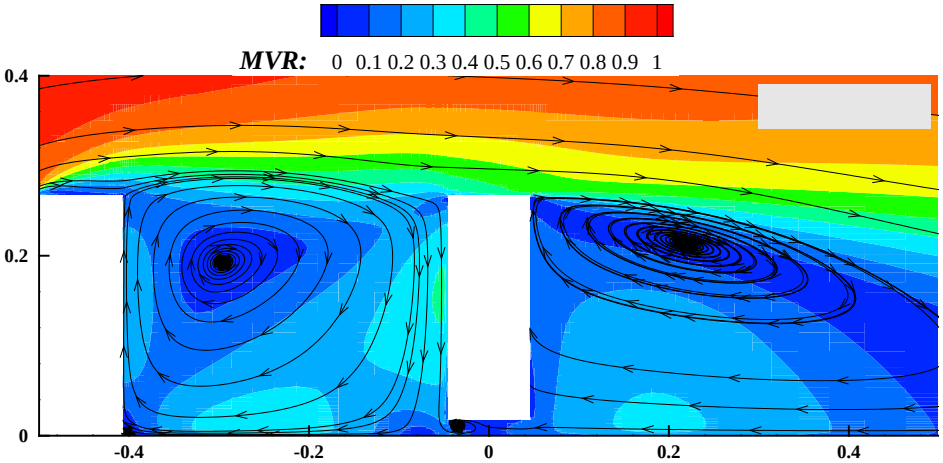
MVR: 0 0.1 0.2 0.3 0.4 0.5 0.6 0.7 0.8 0.9 1
0.4
0.2
0
-0.4
-0.2
0
0.2
0.4

(d)

Fig. 12. MVR and streamlines distribution at the vertical plane of $y = 0$ for (a) Case [DL, 150], (b) Case [DH, 100], (c) Case [DH, 150], and (d) Case [DL, 50].

Fig. 11(c-d) shows area-weighted average MVR ($\overline{\text{MVR}}$) values of lift-up and podium areas for double building models. There is a common phenomenon in both lift-up and podium areas. For cases with the same H_s, case of $(H_T + h)/H_s = 1$ has the minimum $\overline{\text{MVR}}$ value. For the resting two cases of $(H_T + h)/H_s \neq 1$, the one with a taller target building has a greater $\overline{\text{MVR}}$ value. Besides, cases of $(H_T + h)/H_s > 1$ have the maximum $\overline{\text{MVR}}$ values of the lift-up area, which are all over 0.5; cases of $(H_T + h)/H_s < 1$ have the median $\overline{\text{MVR}}$ values, which are all between 0.3 and 0.4; cases of $(H_T + h)/H_s = 1$ have the minimum $\overline{\text{MVR}}$ values, which are all below 0.3. The findings imply that making the target building taller or shorter than the upstream building can both sufficiently improve the overall mean wind velocity of the interest precinct but heightening the target building is more effective. Besides, for cases of $(H_T + h)/H_s = 1$, the $\overline{\text{MVR}}$ value of the lift-up area increases with the building height. It indicates that heightening upstream and target buildings simultaneously can also effectively improve wind comfort in the lift-up area, although it is less effective than only heightening the target building. Nevertheless, heightening upstream and target buildings simultaneously may not necessarily improve wind comfort in the podium. As shown in Figs. 10(c) and 11(d), Case [DM, 100] has the minimum AR_{AWC} value and $\overline{\text{MVR}}$ value of the podium area among three cases of $(H_T + h)/H_s = 1$.

4.2.3. Influences of upstream buildings

From Figs .8(c) and 11(c), it can be observed that cases of double building models always have smaller $\overline{\text{MVR}}$ values of the lift-up area than cases of single building models when they have the same H_T. Therefore, the existence of the upstream building always impairs wind

561 comfort in the lift-up area. Nevertheless, it does not necessarily apply to wind comfort in the
562 podium. As shown in Figs.7(c) and 10(c), Case [DM, 50] and Case [DH, 50] have larger
563 acceptable wind comfort zones in the podium than cases of single building models with the
564 same H_T. For the remaining scenarios, the upstream building's existence shrinks the acceptable
565 wind comfort zone of the podium area by a large margin. It can be concluded that, in some
566 cases, the presence of the upstream building may be beneficial for wind comfort in the podium.

567

568 **4.3. Integrated impacts of building height and upstream building on thermal comfort**

569 **4.3.1. PET distributions in summer**

570 Fig.13 shows area ratios of different PET values (or thermal comfort zones) in the podium
571 and lift-up areas in summer for all cases. The area ratio is defined as the area with a specific
572 PET range divided by the total area of the podium area or lift-up area. For instance, the area
573 ratio of the "Hot" thermal comfort zone in the podium equals the ratio of the area with 38 °C <
574 PET ≤ 42 °C to the total area of the podium area. The area with PET > 44 °C is defined as the
575 "intolerable hot" thermal comfort zone in this paper. As shown in Fig. 13(a), most of the
576 podium area is under the "very hot" or "intolerable hot" thermal condition (PET > 42 °C), and
577 the rest belongs to the "hot" thermal comfort zone (38 °C < PET ≤ 42 °C). This finding means
578 that standing in the podium is often very hot for pedestrians on a sunny summer day due to the
579 intensive solar radiation and high temperature. For cases of single building models, the
580 "intolerable hot" thermal comfort zone is expanded as the building becomes taller. Meanwhile,
581 cases of SD models have larger "hot" thermal comfort zones in the podium than cases of SC
582 models. Therefore, isolated lift-up buildings have better thermal comfort under a diverging
583 flow than under a converging flow. For cases of double building models, cases of $(H_T + h)/H_s$
584 = 1 always have the largest "intolerable hot" thermal comfort zone among cases with the same

585 H_s. When the upstream building is as tall as the target building, heightening or shortening the
586 target building can dramatically decrease the "intolerable hot" thermal comfort zone.

587 In contrast to the podium area, pedestrians experience less heat stress in the lift-up area
588 (Fig. 13(b)). For cases of single building models, the "neutral" thermal comfort zone (26 °C <
589 PET ≤ 30 °C) accounts for 90% ~ 100% of the lift-up area. Cases of SC models have "slightly
590 warm" thermal comfort zones (30 °C < PET ≤ 34 °C) in the lift-up area, and the "slightly warm"
591 zones shrink slightly with the increased building height. For cases of double building models,
592 the entire lift-up area is "slightly warm" for pedestrians in the case of $(H_T + h)/H_s = 1$. On the
593 premise of the same H_s and $(H_T + h)/H_s \neq 1$, the case with a taller target building (i.e., Case
594 [DL, 150], Case [DM, 150], and Case [DH, 100]) has a greater "neutral" thermal comfort zone
595 in the lift-up area than another one (i.e., Case [DL, 100], Case [DM, 50], and Case [DH, 50]).
596 Furthermore, cases of single building models always have a larger "neutral" thermal comfort
597 zone than cases of double building models. The results indicate that, in summer, the existence
598 of upstream buildings can degrade thermal comfort in the lift-up area, and making the target
599 building taller or shorter than the upstream building can effectively improve thermal comfort
600 in the lift-up area.

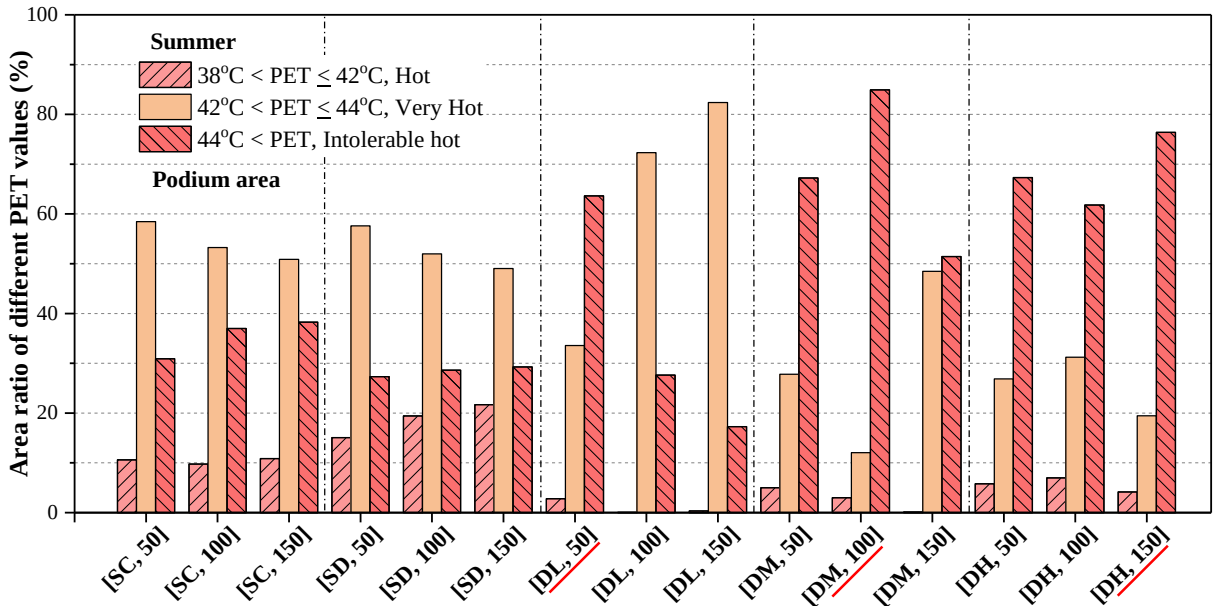

601

(a)

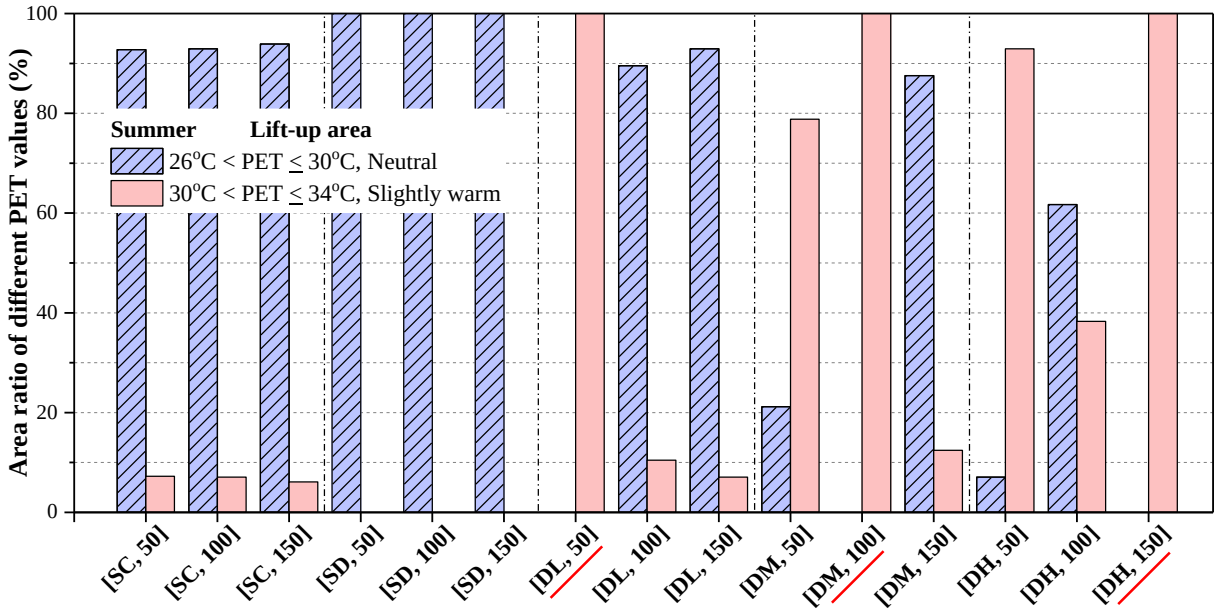

(b)

Fig. 13. Area ratios of different PET values (or thermal comfort zones) in the (a) podium and (b) lift-up areas in summer for all cases.

4.3.2. PET distributions in winter

Fig. 14 shows area ratios of different PET values (or thermal comfort zones) in the podium and lift-up areas in winter for all cases. As shown in Fig. 14(a), the podium area can be divided into four thermal comfort zones based on PET values: “Hot,” “warm,” “slightly warm,” and “neutral.” Although the air temperature is not very high (< 26°C), some places are still hot (PET > 38 °C) for pedestrians in winter due to the low wind velocity and high radiation temperature. For cases of single building models, the size of “neutral” and “slightly warm” thermal comfort zones displays a slight decline tendency with the building height. For cases of DL models, the size of “neutral” and “slightly warm” thermal comfort zones increases as the target building becomes higher. Nevertheless, the variation trend is the opposite among cases

of DH models. As for cases of DM models, Case [DM, 100] has the smallest size of “neutral” and “slightly warm” thermal comfort zones, and Case [DM, 150] has the largest one. In this paper, the “neutral” and “slightly warm” thermal perceptions are assumed to be satisfactory for pedestrians in winter. Therefore, when the target building is as tall as the upstream building, shortening or heightening the target building can effectively improve the podium area’s satisfactory thermal comfort zone in winter.

Contrary to the podium area, the building height and upstream building do not significantly impact the distribution of thermal comfort zones in the lift-up area. As shown in Fig. 14(b), the “cool” thermal comfort zone (18 ˚C < PET ≤ 22 ˚C) almost occupies the entire lift-up area except for Case [DL, 50]. Therefore, in winter, pedestrians often experience moderate cold stress while standing in the lift-up area.

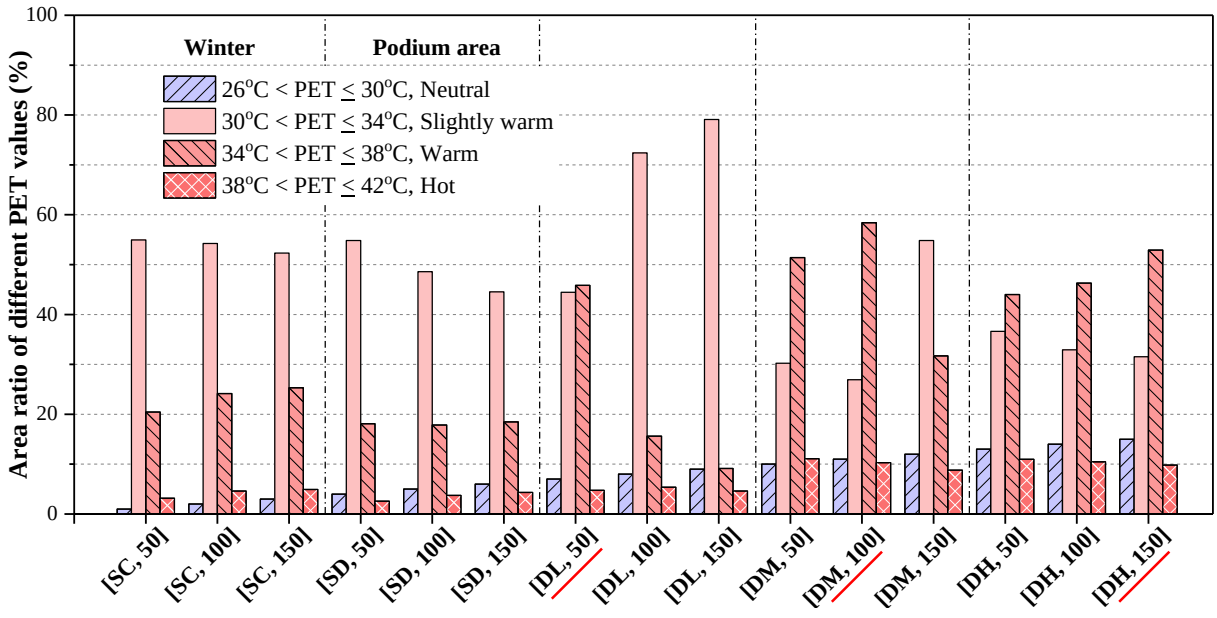

(a)

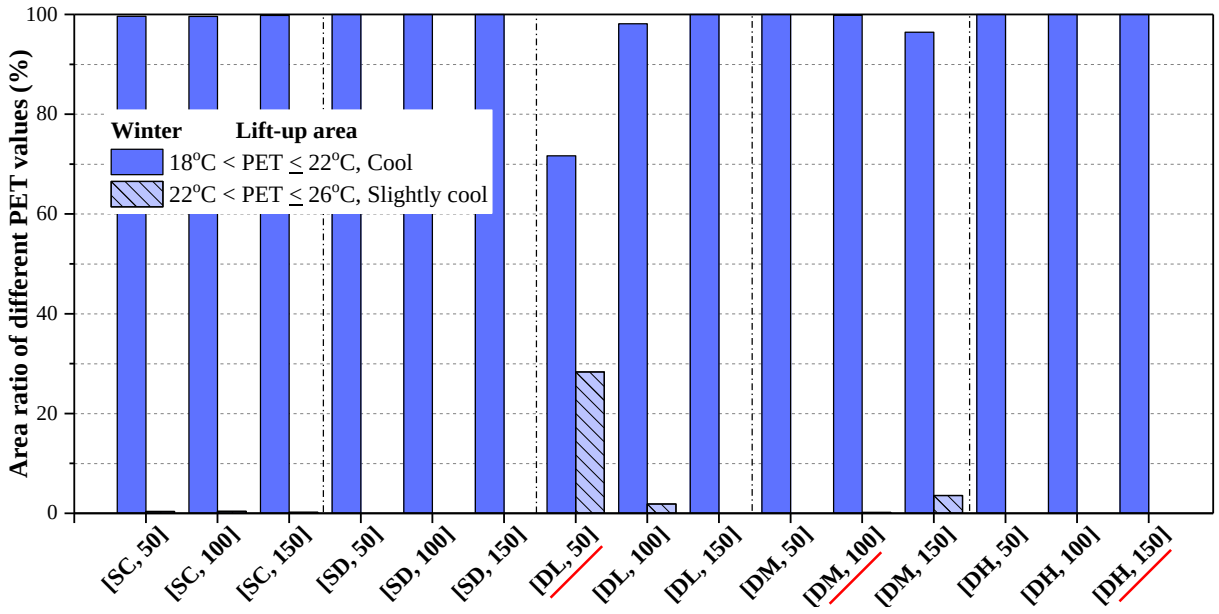

(b)

Fig. 14. Area ratios of different PET values (or thermal comfort zones) in the (a) podium and (b) lift-up areas in winter for all cases.

4.3.3. Area-weighted average PET

The area-weighted average PET ($\overline{PET}$) values of the podium and lift-up areas in summer and winter for all cases are presented in Table 5. The maximum or minimum values are underlined. In summer, the $\overline{PET}$ value of the podium area is between ~43 ˚C and ~45 ˚C, while the $\overline{PET}$ value of the lift-up area is ~29 ˚C to ~31 ˚C. In winter, the $\overline{PET}$ value of the podium area ranges from ~32 ˚C to ~35 ˚C, while the $\overline{PET}$ value of the lift-up area is between ~20 ◦C and ~22 ˚C. Compared to the podium area, the overall PET value in the lift-up area is reduced by over 10 ˚C. Meanwhile, the reduction is more pronounced in summer than in winter.

From Table 5, the following findings can be obtained applicable to both summer and winter. First, cases of SC models have greater $\overline{PET}$ values of the podium and lift-up areas than cases of SD models, indicating that there is a smaller overall PET value when the isolated lift-

up building is under a diverging flow. Second, for cases of double building models, Case [DL, 50], Case [DM, 100], and Case [DH, 150] (i.e., cases of $(H_T + h)/H_s = 1$) have the largest $\overline{PET}$ values (marked in red) of the podium and lift-up areas among cases with the same H_s. Therefore, making the target building taller or shorter than the upstream building can lower the overall PET level in the entire interest precinct. Third, comparing Case [DL, 50], Case [DM, 100], and Case [DH, 150], it can be found that the $\overline{PET}$ value of the lift-up area shows a declining trend with H_T. This indicates that heightening upstream and target buildings simultaneously can decrease the overall PET value in the lift-up area. Last, cases of double building models have larger $\overline{PET}$ values of the lift-up area than cases of single building models with the same H_T, indicating that the existence of upstream buildings increases the lift-up area's overall PET level.

According to Table 2, the PET range for a neutral thermal sensation is between 26 and 30 °C. Hence PET = 28 °C is assumed to be most desirable for pedestrians. When the PET value is below 28 °C, the greater the PET value, the better the thermal comfort; when the PET value is over 28 °C, the smaller the PET value, the better the thermal comfort. Therefore, the effects of building height and upstream building on thermal comfort in the podium do not change between summer and winter as $\overline{PET}$ values are always greater than 28 °C. On the contrary, the impacts of building height and upstream building on thermal comfort in the lift-up area vary with seasons, because $\overline{PET}$ values are over 28 °C in summer but below 28 °C in winter. In summary, for the lift-up area's thermal comfort, making the target building taller or shorter than the upstream building is beneficial in summer but unfavorable in winter. This rule also applies to heightening upstream and target buildings simultaneously. Besides, the existence of upstream buildings is helpful in winter but adverse in summer.

Table 5. Area-weighted average PET ($\overline{PET}$) values of the podium and lift-up areas in summer and winter. (SC and SD: single building models under a converging/diverging flow; DL, DM, and DH: double

building models with H_s = 53.5m, 103.5m, and 153.5m; H_T is the height of lift-up building's main body; H_s is the height of the upstream building.)

$\overline{PET}$ of the podium area in summer	SC	SD	DL	DM	DH
H_T = 50 m	43.54	43.36	44.40	44.64	44.49
H_T = 100 m	43.72	43.35	43.84	44.80	44.40
H_T = 150 m	43.72	43.31	43.44	44.22	44.65
$\overline{PET}$ of the lift-up area in summer	SC	SD	DL	DM	DH
H_T = 50 m	29.45	29.11	31.08	30.14	30.21
H_T = 100 m	29.37	29.00	29.57	30.66	30.06
H_T = 150 m	29.30	28.95	29.39	29.55	30.46
$\overline{PET}$ of the podium area in winter	SC	SD	DL	DM	DH
H_T = 50 m	32.39	32.04	34.13	34.65	34.33
H_T = 100 m	32.75	32.02	32.97	34.98	34.16
H_T = 150 m	32.75	31.96	32.16	33.77	34.66
$\overline{PET}$ of the lift-up area in winter	SC	SD	DL	DM	DH
H_T = 50 m	20.34	20.09	21.96	20.88	20.94
H_T = 100 m	20.29	20.02	20.44	21.41	20.81
H_T = 150 m	20.24	19.98	20.29	20.45	21.18

4.4. Limitation and future work

Despite achieving many significant findings, this study inevitably has some limitations. First, the outcome of this study is based on the slab-like building model and meteorological data measured in Hong Kong. Therefore, results may differ if the building configuration and climate are different from those used in the present study. Second, this study only considers

generic lift-up building models without lift-up cores. The purpose is to highlight the effects of building height and upstream building and eliminate other influential factors like various barriers in the lift-up area, complex and irregular surrounding buildings, and fickle meteorological conditions. The application to a real urban environment should be considered in the future. Third, although this study demonstrates that making the lift-up building taller or shorter than the upstream building can both improve wind comfort and thermal comfort effectively, further investigation is still required to determine the optimum building height. Last, this study limits the research scope to the mean wind velocity using the steady RANS approach. Gust wind is also an important factor influencing pedestrian comfort. Future work will study the influence of building height on gust wind velocity.

5. Conclusions

This study examines the integrated impacts of building height and upstream building on wind comfort and thermal comfort around lift-up buildings using CFD simulations. The mean wind velocity ratio (MVR) and physiological equivalent temperature (PET) were adopted as assessment indices for wind comfort and thermal comfort. Pedestrian-level wind comfort and thermal comfort around two single building models (SC and SD models) and three double building models (DL, DM, and DH models) with three building heights (H_T = 50 m, 100 m, and 150 m) were quantitatively evaluated. The main findings can be summarized as follows:

(1). For single building models, when the lift-up building becomes taller, the acceptable wind comfort zone in the podium (AR_{AWC}) slightly decreases, but corner streams in the lateral zones and throughflow in the lift-up area strengthen. SD models have greater AR_{AWC} and $\overline{\mathrm{MVR}}$ values than SC models with the same H_T. Thus, wind comfort can be improved when the building is under a diverging flow.

(2). For double building models, Case [DL, 50], Case [DM, 100], and Case [DH, 150] have the minimum AR_{AWC} and $\overline{\mathrm{MVR}}$ values among cases with the same upstream building. Therefore, when the upstream building is as tall as the target building, adding or reducing the target building height (i.e., uneven building height) can substantially improve wind comfort in the entire interest precinct. And adding the target building height is more effective.

(3). Double building models have smaller $\overline{\mathrm{MVR}}$ values of the lift-up area than single building models, thus the existence of the upstream building impairs wind comfort in the lift-up area. Besides, heightening the upstream building and target building simultaneously can increase $\overline{\mathrm{MVR}}$ values of the lift-up area, benefiting wind comfort. However, the above rules do not necessarily apply to wind comfort in the podium.

(4). For single building models, area ratios of different thermal comfort zones are not significantly influenced by building height. In contrast, the size of more favorable thermal comfort zones in the podium decreases slightly with the increased building height. Besides, SD models have smaller $\overline{\mathrm{PET}}$ values of the podium and lift-up areas than SC models with the same H_T.

(5). For double building models, Case [DL, 50], Case [DM, 100], and Case [DH, 150] have the minimum $\overline{\mathrm{PET}}$ values among cases with the same upstream building. As $\overline{\mathrm{PET}}$ values of the podium area are always over 28 ◦C, making the target building taller or lower than the upstream building can improve the podium area's thermal comfort in both summer and winter. However, for thermal comfort in the lift-up area, this strategy is only beneficial in summer but unfavorable in winter. This is because $\overline{\mathrm{PET}}$ values of the lift-up area are over 28 ◦C in summer but below 28 ◦C in winter. Heightening upstream and target buildings simultaneously can decrease the $\overline{\mathrm{PET}}$ value of the lift-up area, which is also helpful in summer but detrimental in

winter. On the contrary, the existence of upstream buildings can increase the $\overline{PET}$ value of the lift-up area, which is adverse in summer but advantageous in winter.

This study quantitatively evaluates wind comfort and thermal comfort around the target building from aspects of comfort zones' distribution and area-weighted average values. Such quantitative evaluation methods can be applied to similar issues. The findings enrich the knowledge of how building height influences wind comfort and thermal comfort around lift-up buildings, which can inspire architects and city planners to make good use of building design to create a livable and comfortable residential environment.

Acknowledgments

This work was supported by a Ph.D. studentship funded by The Hong Kong Polytechnic University.

References

[1] J. Li, J. Niu, C.M. Mak, T. Huang, Y. Xie, Assessment of outdoor thermal comfort in Hong Kong based on the individual desirability and acceptability of sun and wind conditions, Building and Environment 145 (2018) 50-61, https://doi.org/10.1016/j.buildenv.2018.08.059.

[2] T. van Druenen, T. van Hooff, H. Montazeri, B. Blocken, CFD evaluation of building geometry modifications to reduce pedestrian-level wind speed, Building and Environment 163 (2019), https://doi.org/10.1016/j.buildenv.2019.106293.

[3] Hong Kong Observatory, Annual average of 12-hourly 10-minute mean wind speed of King's Park and Waglan Island (1968-2015). https://www.hko.gov.hk/en/climate_change/obs_hk_wind.htm.

748 [4] V. Cheng, E. Ng, C. Chan, B. Givoni, Outdoor thermal comfort study in a sub-tropical climate: a
749 longitudinal study based in Hong Kong, International Journal of Biometeorology 56(1) (2012) 43-56,
750 https://doi.org/10.1007/s00484-010-0396-z.
751 [5] J. Niu, J. Liu, T.-c. Lee, Z. Lin, C. Mak, K.-T. Tse, B.-s. Tang, K.C.S. Kwok, A new method to assess
752 spatial variations of outdoor thermal comfort: Onsite monitoring results and implications for precinct
753 planning, Building and Environment 91 (2015) 263-270,
754 https://doi.org/10.1016/j.buildenv.2015.02.017.
755 [6] M. Fan, C.K. Chau, E.H.W. Chan, J. Jia, A decision support tool for evaluating the air quality and
756 wind comfort induced by different opening configurations for buildings in canyons, Science of the Total
757 Environment 574 (2017) 569-582, https://doi.org/10.1016/j.scitotenv.2016.09.083.
758 [7] Y. Du, C.M. Mak, B.S. Tang, Effects of building height and porosity on pedestrian level wind
759 comfort in a high-density urban built environment, Building Simulation 11(6) (2018) 1215-1228,
760 https://doi.org/10.1007/s12273-018-0451-y.
761 [8] Y. Du, C.M. Mak, Improving pedestrian level low wind velocity environment in high-density cities:
762 A general framework and case study, Sustainable Cities and Society 42 (2018) 314-324,
763 https://doi.org/10.1016/j.scs.2018.08.001.
764 [9] C.-Y. Wen, Y.-H. Juan, A.-S. Yang, Enhancement of city breathability with half open spaces in ideal
765 urban street canyons, Building and Environment 112 (2017) 322-336,
766 https://doi.org/10.1016/j.buildenv.2016.11.048.
767 [10] Y.-H. Juan, A.-S. Yang, C.-Y. Wen, Y.-T. Lee, P.-C. Wang, Optimization procedures for
768 enhancement of city breathability using arcade design in a realistic high-rise urban area, Building and
769 Environment 121 (2017) 247-261, https://doi.org/10.1016/j.buildenv.2017.05.035.
770 [11] K.T. Tse, X. Zhang, A.U. Weerasuriya, S.W. Li, K.C.S. Kwok, C.M. Mak, J. Niu, Adopting 'lift-up'
771 building design to improve the surrounding pedestrian-level wind environment, Building and
772 Environment 117 (2017) 154-165, https://doi.org/10.1016/j.buildenv.2017.03.011.
773 [12] L.W. Chew, L.K. Norford, Pedestrian-level wind speed enhancement in urban street canyons with
774 void decks, Building and Environment 146 (2018) 64-76,
775 https://doi.org/10.1016/j.buildenv.2018.09.039.

776 [13] L.W. Chew, L.K. Norford, Pedestrian-level wind speed enhancement with void decks in three-
777 dimensional urban street canyons, Building and Environment 155 (2019) 399-407,
778 https://doi.org/10.1016/j.buildenv.2019.03.058.
779 [14] Q. Xia, X. Liu, J. Niu, K.C.S. Kwok, Effects of building lift-up design on the wind environment
780 for pedestrians, Indoor and Built Environment 26(9) (2015) 1214-1231,
781 https://doi.org/10.1177/1420326x15609967.
782 [15] J. Liu, X. Zhang, J. Niu, K.T. Tse, Pedestrian-level wind and gust around buildings with a 'lift-up'
783 design: Assessment of influence from surrounding buildings by adopting LES, Building Simulation
784 12(6) (2019) 1107-1118, https://doi.org/10.1007/s12273-019-0541-5.
785 [16] Y. Du, C.M. Mak, J. Liu, Q. Xia, J. Niu, K.C.S. Kwok, Effects of lift-up design on pedestrian level
786 wind comfort in different building configurations under three wind directions, Building and
787 Environment 117 (2017) 84-99, https://doi.org/10.1016/j.buildenv.2017.03.001.
788 [17] C. Sha, X. Wang, Y. Lin, Y. Fan, X. Chen, J. Hang, The impact of urban open space and 'lift-up'
789 building design on building intake fraction and daily pollutant exposure in idealized urban models,
790 Science of the Total Environment 633 (2018) 1314-1328,
791 https://doi.org/10.1016/j.scitotenv.2018.03.194.
792 [18] K. Zhang, G. Chen, X. Wang, S. Liu, C.M. Mak, Y. Fan, J. Hang, Numerical evaluations of urban
793 design technique to reduce vehicular personal intake fraction in deep street canyons, Science of the
794 Total Environment 653 (2019) 968-994, https://doi.org/10.1016/j.scitotenv.2018.10.333.
795 [19] K. Zhang, G. Chen, Y. Zhang, S. Liu, X. Wang, B. Wang, J. Hang, Integrated impacts of turbulent
796 mixing and NOX-O3 photochemistry on reactive pollutant dispersion and intake fraction in shallow
797 and deep street canyons, Science of the Total Environment 712 (2020) 135553,
798 https://doi.org/10.1016/j.scitotenv.2019.135553.
799 [20] J. Liu, J. Niu, Q. Xia, Combining measured thermal parameters and simulated wind velocity to
800 predict outdoor thermal comfort, Building and Environment 105 (2016) 185-197,
801 https://doi.org/10.1016/j.buildenv.2016.05.038.

802 [21] T. Huang, J. Li, Y. Xie, J. Niu, C.M. Mak, Simultaneous environmental parameter monitoring and
803 human subject survey regarding outdoor thermal comfort and its modelling, Building and Environment
804 125 (2017) 502-514, https://doi.org/10.1016/j.buildenv.2017.09.015.
805 [22] Y. Du, C.M. Mak, T. Huang, J. Niu, Towards an integrated method to assess effects of lift-up design
806 on outdoor thermal comfort in Hong Kong, Building and Environment 125 (2017) 261-272,
807 https://doi.org/10.1016/j.buildenv.2017.09.001.
808 [23] X. Zhang, K.T. Tse, A.U. Weerasuriya, S.W. Li, K.C.S. Kwok, C.M. Mak, J. Niu, Z. Lin, Evaluation
809 of pedestrian wind comfort near 'lift-up' buildings with different aspect ratios and central core
810 modifications, Building and Environment 124 (2017) 245-257,
811 https://doi.org/10.1016/j.buildenv.2017.08.012.
812 [24] Y. Du, C.M. Mak, Y. Li, A multi-stage optimization of pedestrian level wind environment and
813 thermal comfort with lift-up design in ideal urban canyons, Sustainable Cities and Society 46 (2019),
814 https://doi.org/10.1016/j.scs.2019.101424.
815 [25] Hong Kong Housing Authority, Standard block typical floor plans.
816 https://www.housingauthority.gov.hk/en/global-elements/estate-locator/standard-block-typical-floor-
817 plans/index.html.
818 [26] X. Zhang, K.T. Tse, A.U. Weerasuriya, K.C.S. Kwok, J.l. Niu, Z. Lin, C.M. Mak, Pedestrian-level
819 wind conditions in the space underneath lift-up buildings, Journal of Wind Engineering and Industrial
820 Aerodynamics 179 (2018) 58-69, https://doi.org/10.1016/j.jweia.2018.05.015.
821 [27] L. Chen, C.M. Mak, Numerical evaluation of pedestrian-level wind comfort around "lift-up"
822 buildings with various unconventional configurations, Building and Environment 188 (2021),
823 https://doi.org/10.1016/j.buildenv.2020.107429.
824 [28] Z.T. Ai, C.M. Mak, Potential use of reduced-scale models in CFD simulations to save numerical
825 resources: Theoretical analysis and case study of flow around an isolated building, Journal of Wind
826 Engineering and Industrial Aerodynamics 134 (2014) 25-29,
827 https://doi.org/10.1016/j.jweia.2014.08.009.
828 [29] Y. Tominaga, A. Mochida, R. Yoshie, H. Kataoka, T. Nozu, M. Yoshikawa, T. Shirasawa, AIJ
829 guidelines for practical applications of CFD to pedestrian wind environment around buildings, Journal

of Wind Engineering and Industrial Aerodynamics 96(10-11) (2008) 1749-1761, https://doi.org/10.1016/j.jweia.2008.02.058.

[30] J. Franke, A. Hellsten, H. Schlünzen, B. Carissimo, D. Grawe, I. Goricsán, Z.k. JbHour, A. Karppinen, Best practice guideline for the CFD simulation of flows in the urban environment, 2007.

[31] J. Franke, A. Hellsten, K.H. Schlunzen, B. Carissimo, The COST 732 Best Practice Guideline for CFD simulation of flows in the urban environment: a summary, International Journal of Environment and Pollution 44(1/2/3/4) (2011), https://doi.org/10.1504/ijep.2011.038443.

[32] T.-H. Shih, W.W. Liou, A. Shabbir, Z. Yang, J. Zhu, A new k-ε eddy viscosity model for high reynolds number turbulent flows, Computers & Fluids 24(3) (1995) 227-238, https://doi.org/10.1016/0045-7930(94)00032-t.

[33] B. Blocken, LES over RANS in building simulation for outdoor and indoor applications: A foregone conclusion?, Building Simulation 11(5) (2018) 821-870, https://doi.org/10.1007/s12273-018-0459-3.

[34] B. Blocken, Computational Fluid Dynamics for urban physics: Importance, scales, possibilities, limitations and ten tips and tricks towards accurate and reliable simulations, Building and Environment 91 (2015) 219-245, https://doi.org/10.1016/j.buildenv.2015.02.015.

[35] Fluent, ANSYS FLUENT 13.0 Theory Guide, Turbulence, ANSYS Inc, Canonsburg, PA, 2010.

[36] X.L. Zhang, A.U. Weerasuriya, B. Lu, K.T. Tse, C.H. Liu, Y. Tamura, Pedestrian-level wind environment near a super-tall building with unconventional configurations in a regular urban area, Building Simulation 13(2) (2020) 439-456, https://doi.org/10.1007/s12273-019-0588-3.

[37] X. Zheng, H. Montazeri, B. Blocken, CFD simulations of wind flow and mean surface pressure for buildings with balconies: Comparison of RANS and LES, Building and Environment 173 (2020), https://doi.org/10.1016/j.buildenv.2020.106747.

[38] B. Blocken, J. Carmeliet, Pedestrian wind conditions at outdoor platforms in a high-rise apartment building: generic sub-configuration validation, wind comfort assessment and uncertainty issues, Wind Struct 11(1) (2008) 51-70, https://doi.org/10.12989/was.2008.11.1.051.

[39] B. Blocken, J. Persoon, Pedestrian wind comfort around a large football stadium in an urban environment: CFD simulation, validation and application of the new Dutch wind nuisance standard,

Journal of Wind Engineering and Industrial Aerodynamics 97(5-6) (2009) 255-270, https://doi.org/10.1016/j.jweia.2009.06.007.

[40] A. Ricci, I. Kalkman, B. Blocken, M. Burlando, M.P. Repetto, Impact of turbulence models and roughness height in 3D steady RANS simulations of wind flow in an urban environment, Building and Environment 171 (2020), https://doi.org/10.1016/j.buildenv.2019.106617.

[41] B. Blocken, P. Moonen, T. Stathopoulos, J. Carmeliet, Numerical Study on the Existence of the Venturi Effect in Passages between Perpendicular Buildings, J Eng Mech 134(12) (2008) 1021-1028, https://doi.org/10.1061/(Asce)0733-9399(2008)134:12(1021).

[42] H. Mittal, A. Sharma, A. Gairola, Numerical simulation of pedestrian level wind flow around buildings: Effect of corner modification and orientation, Journal of Building Engineering 22 (2019) 314-326, https://doi.org/10.1016/j.jobe.2018.12.014.

[43] B. Blocken, W.D. Janssen, T. van Hooff, CFD simulation for pedestrian wind comfort and wind safety in urban areas: General decision framework and case study for the Eindhoven University campus, Environmental Modelling & Software 30 (2012) 15-34, https://doi.org/10.1016/j.envsoft.2011.11.009.

[44] W.D. Janssen, B. Blocken, T. van Hooff, Pedestrian wind comfort around buildings: Comparison of wind comfort criteria based on whole-flow field data for a complex case study, Building and Environment 59 (2013) 547-562, https://doi.org/10.1016/j.buildenv.2012.10.012.

[45] R. Meroney, Wind tunnel and numerical simulation of pollution dispersion: a hybrid approach, Paper for Invited Lecture at the Croucher Advanced Study Institute, Hong Kong University of Science and Technology (2004) 6-10,

[46] B.E. Launder, D.B. Spalding, The numerical computation of turbulent flows, Computer Methods in Applied Mechanics and Engineering 3(2) (1974) 21, https://doi.org/https://doi.org/10.1016/0045-7825(74)90029-2.

[47] T. Cebeci, P. Bradshaw, Momentum transfer in boundary layers, Washington (1977).

[48] B. Blocken, T. Stathopoulos, J. Carmeliet, CFD simulation of the atmospheric boundary layer: wall function problems, Atmospheric Environment 41(2) (2007) 238-252, https://doi.org/10.1016/j.atmosenv.2006.08.019.

885 [49] E. Ng, Policies and technical guidelines for urban planning of high-density cities - air ventilation
886 assessment (AVA) of Hong Kong, Building and Environment 44(7) (2009) 1478-1488,
887 https://doi.org/10.1016/j.buildenv.2008.06.013.
888 [50] Y. Du, C.M. Mak, Y. Li, Application of a multi-variable optimization method to determine lift-up
889 design for optimum wind comfort, Building and Environment 131 (2018) 242-254,
890 https://doi.org/10.1016/j.buildenv.2018.01.012.
891 [51] Y. Du, C.M. Mak, K. Kwok, K.-T. Tse, T.-c. Lee, Z. Ai, J. Liu, J. Niu, New criteria for assessing
892 low wind environment at pedestrian level in Hong Kong, Building and Environment 123 (2017) 23-36,
893 https://doi.org/10.1016/j.buildenv.2017.06.036.
894 [52] NEN, Wind comfort and wind danger in the built environment, Netherlands Normalisation Institute,
895 NEN8100 (in Dutch), 2006.
896 [53] F. Binarti, M.D. Koerniawan, S. Triyadi, S.S. Utami, A. Matzarakis, A review of outdoor thermal
897 comfort indices and neutral ranges for hot-humid regions, Urban Climate 31 (2020),
898 https://doi.org/10.1016/j.uclim.2019.100531.
899 [54] P. Kumar, A. Sharma, Study on importance, procedure, and scope of outdoor thermal comfort –A
900 review, Sustainable Cities and Society 61 (2020), https://doi.org/10.1016/j.scs.2020.102297.
901 [55] P. Hoppe, The physiological equivalent temperature - a universal index for the biometeorological
902 assessment of the thermal environment, International Journal of Biometeorology 43(2) (1999) 71-5,
903 https://doi.org/10.1007/s004840050118.
904 [56] T.P. Lin, A. Matzarakis, Tourism climate and thermal comfort in Sun Moon Lake, Taiwan,
905 International Journal of Biometeorology 52(4) (2008) 281-90, https://doi.org/10.1007/s00484-007-
906 0122-7.
907 [57] A. Matzarakis, Rutz, F., Mayer, H., Modelling Radiation fluxes in simple and complex
908 environments – Application of the RayMan model, International Journal of Biometeorology 51 (2007)
909 12.
910 [58] A. Matzarakis, Rutz, F., Mayer, H., Modelling Radiation fluxes in simple and complex
911 environments – Basics of the RayMan model, International Journal of Biometeorology 54 (2010) 9.

912 [59] E. Willemsen, J.A. Wisse, Design for wind comfort in The Netherlands: Procedures, criteria and
913 open research issues, Journal of Wind Engineering and Industrial Aerodynamics 95(9-11) (2007) 1541-
914 1550, https://doi.org/10.1016/j.jweia.2007.02.006.
915 [60] ASHRAE, ASHRAE Standard 55: Thermal Environmental Conditions for Human Occupancy,
916 ASHRAE, 2013, p. 54.
917 [61] J. Liu, J. Niu, C.M. Mak, Q. Xia, Detached eddy simulation of pedestrian-level wind and gust
918 around an elevated building, Building and Environment 125 (2017) 168-179,
919 https://doi.org/10.1016/j.buildenv.2017.08.031.
920 [62] B. Blocken, T. Stathopoulos, J.P.A.J. van Beeck, Pedestrian-level wind conditions around buildings:
921 Review of wind-tunnel and CFD techniques and their accuracy for wind comfort assessment, Building
922 and Environment 100 (2016) 50-81, https://doi.org/10.1016/j.buildenv.2016.02.004.
923 [63] B. Blocken, 50 years of Computational Wind Engineering: Past, present and future, Journal of
924 Wind Engineering and Industrial Aerodynamics 129 (2014) 69-102,
925 https://doi.org/10.1016/j.jweia.2014.03.008.
926 [64] Y. Tominaga, A. Mochida, S. Murakami, S. Sawaki, Comparison of various revised k–ε models
927 and LES applied to flow around a high-rise building model with 1:1:2 shape placed within the surface
928 boundary layer, Journal of Wind Engineering and Industrial Aerodynamics 96(4) (2008) 389-411,
929 https://doi.org/10.1016/j.jweia.2008.01.004.
930 [65] S.D. Sabatino, R. Buccolieri, H.R. Olesen, M. Ketzel, R. Berkowicz, J. Franke, M. Schatzmann,
931 K.H. Schlunzen, B. Leitl, R. Britter, C. Borrego, A.M. Costa, S.T. Castelli, T.G. Reisin, A. Hellsten, J.
932 Saloranta, N. Moussiopoulos, F. Barmpas, K. Brzozowski, I. Goricsan, M. Balczo, J.G. Bartzis, G.
933 Efthimiou, J.L. Santiago, A. Martilli, M. Piringer, K.B. Stanzer, M. Hirtl, A.A. Baklanov, R.B.
934 Nuterman, A.V. Starchenko, COST 732 in practice: the MUST model evaluation exercise, International
935 Journal of Environment and Pollution 44(1/2/3/4) (2011), https://doi.org/10.1504/ijep.2011.038442.
936 [66] H.O. Michael Schatzmann, Jörg Franke, COST 732 Model Evaluation Case Studies: Approach and
937 Results, COST Office, Brussels, Belgium, 2010.

[67] S.R. Hanna, O.R. Hansen, S. Dharmavaram, FLACS CFD air quality model performance evaluation with Kit Fox, MUST, Prairie Grass, and EMU observations, Atmospheric Environment 38(28) (2004) 4675-4687, https://doi.org/10.1016/j.atmosenv.2004.05.041.

[68] Y. Tamura, X. Xu, Q. Yang, Characteristics of pedestrian-level Mean wind speed around square buildings: Effects of height, width, size and approaching flow profile, Journal of Wind Engineering and Industrial Aerodynamics 192 (2019) 74-87, https://doi.org/10.1016/j.jweia.2019.06.017.